

Entangling color centers via magnon-antimagnon pair creation

Eric Kleinherbers,^{*} Shane P. Kelly, and Yaroslav Tserkovnyak

*Department of Physics and Astronomy and Bhauvik Institute for Theoretical Physics,
University of California, Los Angeles, California 90095, USA*

(Dated: November 18, 2024)

We present how entanglement between a spatially separated pair of color centers can be created by letting them weakly interact with the quantum fluctuations of a nonequilibrium magnetic environment. To this end, we consider two coupled ferromagnets, one in the ground state and one in an inverted state with respect to an applied magnetic field. The resulting energetic instability leads to a quantum spin current in the vacuum state that is sustained by the creation of magnon-antimagnon pairs at the interface. We show that these quantum fluctuations imprint a steady-state entanglement onto the two dipole-coupled color centers through nonlocal dissipation. We derive conditions for establishing a maximally entangled Bell state. This entanglement is absent in thermal equilibrium.

Introduction.—Engineering entanglement between qubits is a common goal in all of quantum science as it is key for quantum advantage in sensing, computation, and communication. Embedding qubits into a solid-state environment [1–6] has potential to advance this endeavor due to the plethora of environments available to engineer nonlocal correlations through electronic and spintronic control. Here, our goal is to imprint these correlations onto weakly coupled qubits in the form of entanglement through natural dissipative evolution [7]. For qubits, we consider color centers (e.g., nitrogen-vacancy centers), which are used as pristine tools for magnetometry [8] and relaxometry [9] even at room temperature.

A necessary condition for creating *steady-state* entanglement between independent qubits that are weakly coupled through an environment is to drive the environment out of equilibrium. This is because in equilibrium — irrespective of how strong the environment correlations are — detailed balance will always enforce an uncorrelated Gibbs state [10]. Only transient entanglement generation may occur [7]. Therefore, we consider in this Letter the *nonequilibrium* magnetic environment shown in Fig. 1(a), which was studied in Ref. [11] as a magnonic version of the bosonic Klein paradox [12, 13]. A ground-state ferromagnet (left) is weakly coupled to the interface to an *inverted-state* ferromagnet (right), where the former is aligned and the latter is antialigned with the applied magnetic field. To avoid the instability, the inverted system is dynamically stabilized by a spin torque [11].

Conceptually, the physics is similar to an analog black hole [14, 15], where the horizon is mimicked by the interface between the stable and the unstable magnet with positive and negative excitation energies, respectively. Due to quantum fluctuations, this instability can be harvested through magnon pair production that is reminiscent of Hawking radiation. Here, the pair creation sustains a purely quantum spin current consisting of positive-energy magnons with $+\hbar$ emitted to the left and negative-energy magnons (or antimagnons [16]) with $-\hbar$ emitted to the right.

Our main result is demonstrating that two color cen-

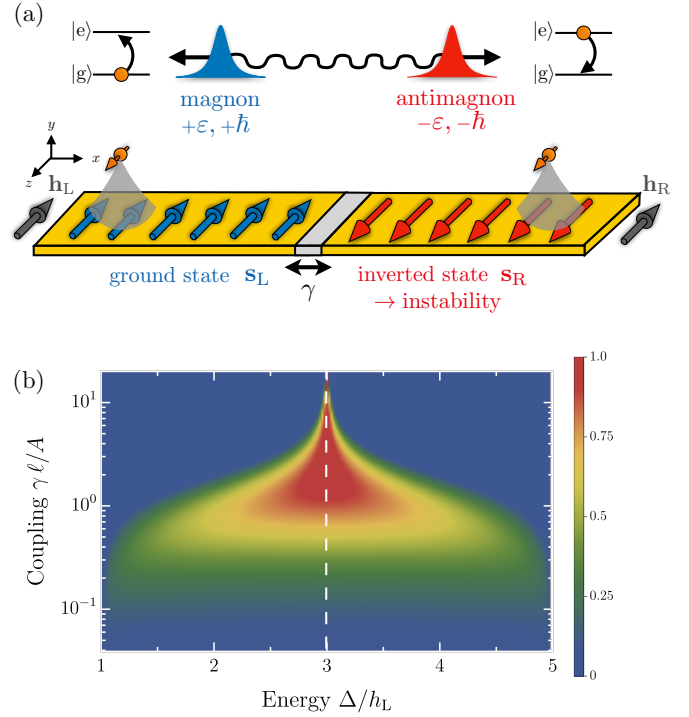


FIG. 1. (a) Setup for magnon-antimagnon pair creation at the interface between two ferromagnets, one in the ground state (left) and one in the inverted state (right). The ferromagnets are magnetically coupled to color centers (orange arrows) that can absorb the generated magnon-antimagnon pairs and become entangled with each other. (b) Steady-state concurrence \mathcal{C} (an entanglement measure) as a function of the color center energy Δ and the interfacial coupling γ . We choose $h_R = 5h_L$ and define the length scale $\ell = \sqrt{A/(h_R - h_L)}$.

ters, placed in proximity of the two magnets, pick up the entanglement of the magnon-antimagnon pairs in the nonequilibrium steady state. The anisotropic magneto-static coupling between the dipole moments of the color centers and the stray field of the magnets turns out to be beneficial, as it facilitates a perfectly chiral coupling and eliminates dephasing. We derive a Lindblad mas-

ter equation with nonlocal gain and loss and find that in the steady state, the color centers become entangled, see Fig. 1(b). The concurrence \mathcal{C} [17], used as a measure of entanglement, is close to one in a sweet spot (red) tuned by the color center energy Δ and the weak interfacial exchange coupling strength γ . Along the symmetry axis (white dashed line), the steady state becomes pure and is of the simple form

$$|\psi\rangle = \frac{r|g,e\rangle - t|e,g\rangle}{\sqrt{r^2 + t^2}}, \quad (1)$$

where g and e denote the ground and the excited state of the two color centers.

Here, r and t are scattering amplitudes describing the pair creation in the environment (see details below). They are obtained from a generalized (nonunitary) scattering theory [14] using a bosonic Bogoliubov ansatz for both positive-energy and negative-energy magnons. The scattering amplitudes fulfill $r^2 - t^2 = 1$. For zero interfacial coupling, $\gamma = 0$, the production of magnon-antimagnon pairs is zero, which leads to $t = 0$ and $r = 1$. In this limit, we obtain the unentangled steady state $|\psi\rangle = |g,e\rangle$, where the spontaneous emission of a negative-energy magnon triggers a population inversion on the right side. As the coupling is turned on, $\gamma > 0$, entangled magnon pairs are produced, $t > 0$, and can nonlocally excite the color centers through dissipative coupling. In the limit $r \approx t \gg 1$, the steady state approaches the Bell state $|\psi\rangle \approx (|g,e\rangle - |e,g\rangle)/\sqrt{2}$.

Nonequilibrium magnetic environment.—We model the nonequilibrium magnetic environment via the Hamiltonian $H_E = \int dx (\mathcal{H}_L + \mathcal{H}_R + \mathcal{H}_I)$ that consists of contributions from the left ground-state ferromagnet, the right inverted-state ferromagnet, and the coupling at the interface (see Fig. 1). In the absence of \mathcal{H}_I , the spin density \mathbf{s}_L of the left side is in the ground state, $\langle \mathbf{s}_L \rangle = -s\mathbf{e}_z$, aligned with the external field $\mathbf{h}_L = -h_L\mathbf{e}_z/\hbar$, where s is the spin density per length. On the right side, the spin density \mathbf{s}_R is in the *inverted state*, $\langle \mathbf{s}_R \rangle = +s\mathbf{e}_z$, antialigned with the external field $\mathbf{h}_R = -h_R\mathbf{e}_z/\hbar$. This inverted state is unstable, since dissipation through Gilbert damping will relax the magnet to its ground state. A dynamical stabilization is achieved, for example, by pumping the inverted magnet through spin torques with a spin accumulation $\mu < -h_R$ below the magnon band [see red dashed line in Fig. 2(b)].

The degrees of freedom of this environment are captured by the magnonic field operators ψ_L and ψ_R with spin $+\hbar$ and $-\hbar$ on top of the ground ($x < 0$) and the inverted state ($x > 0$), respectively. They are defined via the usual linearized Holstein-Primakoff relations $\sqrt{2\hbar s}\psi_L \approx s_L^x - is_L^y$ and $\sqrt{2\hbar s}\psi_R \approx s_R^x + is_R^y$. Their dynamics in the bulk are described by the Hamiltonians

$$\mathcal{H}_\alpha = A (\partial_x \psi_\alpha^\dagger) (\partial_x \psi_\alpha) \pm h_\alpha \psi_\alpha^\dagger \psi_\alpha, \quad (2)$$

where $\alpha \in L, R$. The first term reflects the bulk exchange interaction with spin stiffness A that favors a parallel alignment of the spins. The second term is the Zeeman energy. The resulting bulk excitation energies of the magnons are given by $\varepsilon_{L,R} = Ak^2 \pm h_{L,R}$ (see blue lines in Fig. 2) as a function of the wavenumber k . The magnon energies are raised by h_L in the left magnet, while they are lowered by h_R in the right magnet. As a result, we obtain negative excitation energies, $\varepsilon_R < 0$, which indicates the instability of the inverted magnet.

Generation of entangled magnon-antimagnon pairs occurs when the inverted magnet — which acts as a source of energy — is coupled at the interface to the normal magnet. We assume an exchange coupling $\sim \mathbf{s}_L \cdot \mathbf{s}_R$ that couples the left and right magnons via

$$\mathcal{H}_I = \gamma \delta(x) \left(\psi_L^\dagger \psi_L + \psi_R^\dagger \psi_R + \psi_R \psi_L + \psi_L^\dagger \psi_R^\dagger \right), \quad (3)$$

where γ is the exchange coupling strength. In a linear treatment of the spin fluctuations, the sign of γ is irrelevant. Also, we are interested in the regime of a weak link, where the microscopic exchange energy is much weaker at the interface than in the bulk. Crucially, \mathcal{H}_I contains the pair creation term $\sim \delta(x)\psi_L^\dagger\psi_R^\dagger$ that becomes resonant when positive-energy magnons in the left magnet [blue filled dots in Fig. 2(a)] are matched with negative-energy magnons in the right magnet [red dots in Fig. 2(b)]. This can only happen for energies in the interval $h_L < \varepsilon_L < h_R$ (blue shaded area) and $-h_R < \varepsilon_R < -h_L$ (red shaded area). Thus, we require $h_R - h_L > 0$. The last two terms of Eq. (3) generate two-mode squeezing similar to photon pair creation in parametric amplifiers [18, 19].

Magnon-antimagnon pair creation.—Production of entangled magnon-antimagnon pairs is described by a generalized (nonunitary) scattering theory in a bosonic Bogoliubov space. The calculations are performed in analogy to Ref. [14], where Hawking radiation of phonons in acoustic black holes is investigated. Expanding the magnon field operators in terms of in-scattering states, we obtain [20]

$$\begin{aligned} \psi_L(x) &= \int_{h_L}^{h_R} \frac{d\varepsilon}{\sqrt{h\nu_L}} \left[(e^{iq_L x} + r_a e^{-iq_L x}) a_\varepsilon + t_b e^{-iq_L x} b_{-\varepsilon}^\dagger \right], \\ \psi_R(x) &= \int_{-h_R}^{-h_L} \frac{d\varepsilon}{\sqrt{h\nu_R}} \left[(e^{-iq_R x} + r_b e^{iq_R x}) b_\varepsilon + t_a e^{iq_R x} a_{-\varepsilon}^\dagger \right], \end{aligned} \quad (4)$$

where $h = 2\pi\hbar$ is the Planck constant. The operators a_ε and b_ε describe the two relevant in-scattering solutions with $[a_\varepsilon, a_{\varepsilon'}^\dagger] = [b_\varepsilon, b_{\varepsilon'}^\dagger] = \delta(\varepsilon - \varepsilon')$ [see Fig. 2(a)-(c)]. The scattering mode a_ε describes an incident positive-energy magnon from the left with amplitude one that gets reflected with amplitude $r_a(\varepsilon)$ and transmitted as a negative-energy magnon with amplitude

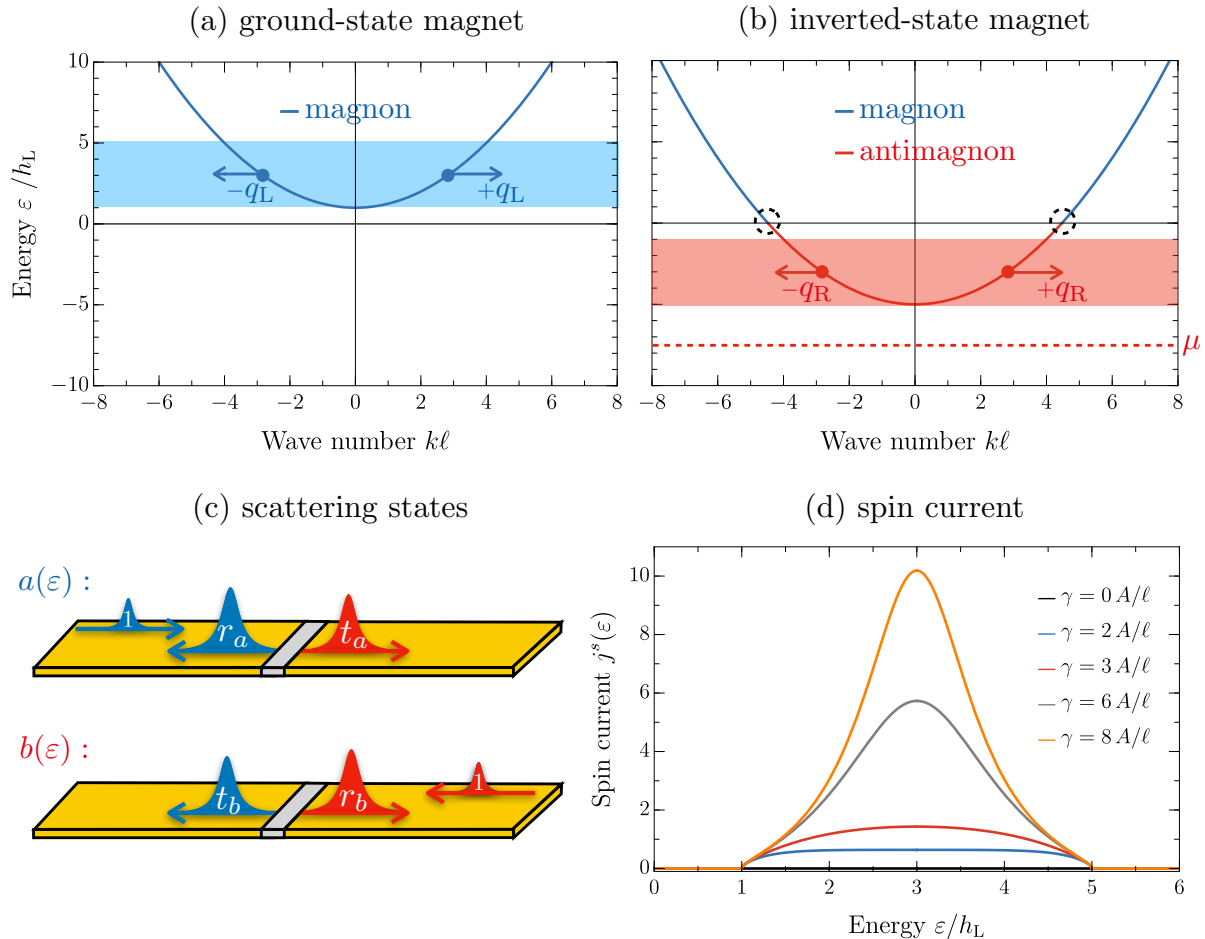


FIG. 2. (a)-(b) Magnon excitation energies $\varepsilon_{L,R}$ for the left ground-state magnet (blue lines) and the right inverted-state magnet (red line). For energies $h_L < \varepsilon_L < h_R$ (blue area on the left) and $-h_R < \varepsilon < -h_L$ (red area on the right) magnons with positive and negative energy can be created pairwise at the interface. The dashed circles indicate the zero-energy magnons that potentially can induce dephasing. (c) Sketch of the scattering states $a(\varepsilon)$ and $b(\varepsilon)$. (d) The magnon pair creation sustains a spin current $j^s(\varepsilon)$ in the vacuum state $|\Omega\rangle$, which is flowing to the left. The current is only nonzero for energies $h_L < \varepsilon < h_R$. The stronger the coupling γ at the interface, the more pairs are emitted. The parameters are the same as in Fig. 1.

$t_a(\varepsilon)$ [see Fig. 2(c)]. Scattering into positive-energy magnons on the right is not allowed by spin conservation. Similarly, the scattering mode b_ε describes an incident negative-energy magnon from the right with amplitude one that gets reflected with amplitude $r_b(\varepsilon)$ and transmitted as a positive-energy magnon with amplitude $t_b(\varepsilon)$ [see Fig. 2(c)]. The wave numbers are given by $q_L = \sqrt{(\varepsilon - h_L)/A}$ and $q_R = \sqrt{(\varepsilon + h_R)/A}$ with group velocities $v_L = 2Aq_L/\hbar$ and $v_R = 2Aq_R/\hbar$, respectively. We remark that the expansion from Eq. (4) is incomplete as higher-energy scattering solutions are omitted. These scattering states are irrelevant for our findings below but are fully accounted for in the Supplemental Material [20], where we also give the specific form of the scattering amplitudes.

The scattering amplitudes from Eq. (4) can be com-

pactly encoded in the scattering matrix:

$$S = \begin{pmatrix} r_a(\varepsilon) & t_b(\varepsilon) \\ t_a^*(-\varepsilon) & r_b^*(-\varepsilon) \end{pmatrix}, \quad (5)$$

where S relates the in-scattering states $(a_\varepsilon, b_{-\varepsilon}^\dagger)$ to their corresponding out-scattering counterparts. The full energy dependence of S is determined from the matching conditions at the interface described by Eq. (3). Importantly, the scattering matrix is not unitary but fulfills $S\tau_z S^\dagger = \tau_z$ with Pauli matrix τ_z in order to maintain the bosonic commutation relations of a_ε and $b_{-\varepsilon}^\dagger$. In addition, there exists an effective time reversal symmetry $SS^* = \mathbf{1}$. It directly follows that $|t_a(-\varepsilon)| = |t_b(\varepsilon)| \equiv t$, $|r_a(\varepsilon)| = |r_b(-\varepsilon)| \equiv r$, as well as $r^2 - t^2 = 1$. The last relation lies at the heart of the bosonic Klein paradox [12, 13], where the nonunitarity of S can enhance both the reflection and the transmission amplitudes,

$r > t > 1$. In contrast, for conventional scattering problems, unitarity enforces $r^2 + t^2 = 1$.

Having solved for the magnon operators, we can determine the spin current due to the spontaneous pair production via

$$\hat{I}_\alpha^s(x) = \pm 2A [\psi_\alpha^\dagger (-i\partial_x \psi_\alpha) - (-i\partial_x \psi_\alpha^\dagger) \psi_\alpha], \quad (6)$$

where the + and the - sign holds for $\alpha = L$ and $\alpha = R$, respectively. Even in the vacuum state defined through

$$a(\varepsilon) |\Omega\rangle = b(\varepsilon) |\Omega\rangle = 0, \quad (7)$$

the system sustains a spin current that is flowing to the left:

$$\langle \Omega | \hat{I}_\alpha^s(x) | \Omega \rangle = -\frac{1}{\pi} \int_{h_L}^{h_R} d\varepsilon t(\varepsilon)^2. \quad (8)$$

Here, the prefactor follows from $2\hbar/h$, where each magnon carries the spin \hbar , in analogy to the electron current in the Landauer-Büttiker formalism [21]. The spin current is purely quantum as it originates in the vacuum fluctuations at the interface. It only flows in the energy window $h_L < \varepsilon < h_R$ and it corresponds to the constant creation of magnon-antimagnon pairs, where $+\hbar$ magnons with positive energy move to the left and $-\hbar$ magnons with negative energy (or antimagnons) move to the right. In Fig. 2(d), we show the energy-resolved spin current $j^s(\varepsilon) = t^2/\pi$ as a measure of the spontaneous pair emission spectrum. The emission occurs symmetrically with respect to $\varepsilon = (h_L + h_R)/2$. A significant change of the spin current j^s occurs as the exchange coupling γ is varied on the characteristic scale A/ℓ with $\ell = \sqrt{A/(h_R - h_L)}$. In a microscopic Heisenberg model, this characteristic value $\gamma \sim A/\ell$ translates to $J'\ell \sim Ja$, where J and J' are the bulk and interfacial exchange energies and a is the atomic lattice constant. Since $\ell \gg a$, a weak link with $J' \ll J$ is sufficient to enable spontaneous pair emission with $j^s \sim \mathcal{O}(1)$. In a recent work [22], the current-current correlations were analyzed to investigate the entanglement between magnons and antimagnons.

Imprinting entanglement.—To sense the pair creation, we couple two color centers to the magnet. Their bare Hamiltonian is given by $H_S = -\Delta\sigma_L^z/2 - \Delta\sigma_R^z/2$, with $\Delta > 0$, using the Pauli matrices σ_α^j labeled by $j \in x, y, z$. Thus, energetically both color centers favor the $+z$ direction, with ground state $|g, g\rangle$. The basis states are denoted by $|g, g\rangle, |g, e\rangle, |e, g\rangle$ and $|e, e\rangle$ with g and e standing for the ground and the excited state, respectively.

The color centers interact with the stray field \mathbf{h}_s of the environment through the magnetostatic coupling Hamiltonian

$$H_C = -\frac{\hbar}{2} \sum_{\alpha=L,R} \left[h_s^+(\mathbf{r}_\alpha) \sigma_\alpha^- + h_s^-(\mathbf{r}_\alpha) \sigma_\alpha^+ + h_s^z(\mathbf{r}_\alpha) \sigma_\alpha^z \right], \quad (9)$$

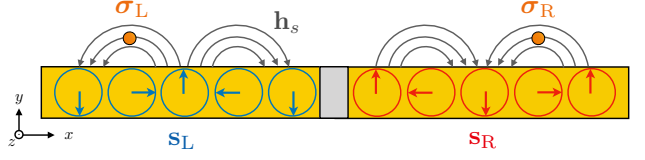


FIG. 3. Snapshot of Halbach-like stray field \mathbf{h}_s from the magnetic excitations described by \mathbf{s}_L and \mathbf{s}_R . The stray magnetic field is only created above the magnet if magnons are moving to the left (right) on the left (right) side. In addition, a combination of time reversal symmetry and mirror symmetry in the xy plane ensures $h_s^z = 0$.

where we introduced $\sigma_\alpha^\pm = (\sigma_\alpha^x \pm i\sigma_\alpha^y)/2$ and $h_s^\pm = h_s^x \pm ih_s^y$. Here, $\mathbf{r}_\alpha = (x_\alpha, d, 0)$ denotes the position of the color centers at height $d > 0$ on either side of the interface with $x_L < 0$ and $x_R > 0$ (see Fig. 1). The stray field \mathbf{h}_s can be calculated via the magnetostatic Greens function [23], where its source are the magnonic excitations described by ψ_L and ψ_R of Eq. (4).

Generically, the anisotropy of the magnetostatic coupling from Eq. (9) is expected to be a nuisance, as it spoils the spin z symmetry and can lead to magnon-induced dephasing [which is resonant at zero energy and therefore energetically enabled by the instability in the right magnet, see dashed circles in Fig. 2(b)]. However, in our setup, the coupling turns out to be beneficial for two reasons. First, due to a combination of time-reversal and xy mirror symmetry of the magnonic spin excitations (see Fig. 3), it follows that $h_s^z = 0$. This eliminates magnon-induced dephasing of the color centers. Second, as shown in Fig. 3, the stray field of a single magnon is Halbach array-like [24], so it is nonzero either only above or below the magnet depending on its wave vector k . In order to be sensitive to the pair creation, we want the left color center to couple to left-moving positive-energy magnons ($k = -q_L$) and the right color center to couple to right-moving negative-energy magnons ($k = +q_R$). For $|x_\alpha| \gg d$, we obtain [20]

$$h_s^+(\mathbf{r}_L) \propto \int_{h_L}^{h_R} \frac{d\varepsilon}{\sqrt{\hbar v_L}} q_L e^{-q_L d} e^{-iq_L x_L} \left(r_a a_\varepsilon + t_b b_{-\varepsilon}^\dagger \right), \quad (10)$$

$$h_s^-(\mathbf{r}_R) \propto \int_{-h_R}^{-h_L} \frac{d\varepsilon}{\sqrt{\hbar v_R}} q_R e^{-q_R d} e^{iq_R x_R} \left(r_b b_\varepsilon + t_a a_{-\varepsilon}^\dagger \right). \quad (11)$$

Thus, the dipole coupling has introduced the typical filter function $q_L e^{-q_L d}$ and $q_R e^{-q_R d}$ [23, 25]. In addition, the chirality has eliminated the incoming plane waves with amplitude one from Eq. (4).

Integrating out the environment degrees of freedom a_ε and b_ε in the effective vacuum state $|\Omega\rangle$, we obtain a

Lindblad master equation for the reduced density matrix ρ in a Born-Markov treatment [20]

$$\partial_t \rho = \frac{1}{i\hbar} [H_S + \delta H, \rho] + \sum_{i=1}^2 \Gamma_0 \left(L_i \rho L_i^\dagger - \frac{1}{2} \{L_i^\dagger L_i, \rho\} \right), \quad (12)$$

where the rate is given by $\Gamma_0 = \gamma_e^4 \hbar^2 s / W^2 A d$ in Gaussian units with the gyromagnetic ratio γ_e and the width of the magnetic strip W . The magnetic fluctuations encoded in Greens functions of $h_s^+(\mathbf{r}_\alpha)$ and $h_s^-(\mathbf{r}_\alpha)$ generically induce both nonlocal coherent dynamics described by δH as well as nonlocal dissipative dynamics described by the Lindblad operators L_1 and L_2 . By using the properties $S\tau_z S^\dagger = \tau_z$ and $SS^* = \mathbb{1}$ of the nonunitary scattering matrix, it can be shown that $\delta H = 0$ [26]. For the nonlocal dissipation, we obtain the Lindblad operators

$$L_1 = \sqrt{q_L d} e^{-q_L d} r \sigma_L^+ + \sqrt{\bar{q}_R d} e^{-\bar{q}_R d} t \sigma_R^+, \quad (13)$$

$$L_2 = \sqrt{q_L d} e^{-q_L d} t \sigma_L^- + \sqrt{\bar{q}_R d} e^{-\bar{q}_R d} r \sigma_R^-, \quad (14)$$

where all functions are evaluated at the resonant energy $\varepsilon = \Delta$ and we define $\bar{q}_R(\Delta) = q_R(-\Delta)$. In addition, we performed local z rotations to obtain the real amplitudes r and t . The dependence on the positions of the color centers x_α has disappeared due to the chiral nature of the coupling.

The Lindblad operator L_1 (L_2) describes the emission (absorption) of a positive-energy magnon on the left side paired with the absorption (emission) of a negative-energy magnon on the right side, with both processes decreasing (increasing) the energy of the color centers. In the limit of no pair creation, $\gamma \rightarrow 0$, we obtain $r = 1$ and $t = 0$. Then, L_1 and L_2 trigger the spontaneous emission of a positive-energy magnon on the left side and a negative-energy on the right side. Thus, the steady state of the color centers becomes $|g, e\rangle$, where on the right side a population inversion is created akin to negative temperature. For finite coupling, $\gamma > 0$, magnon-antimagnon pairs are produced, which enables both absorption with $t > 0$ and stimulated emission with $r > 1$. Then, the environment can imprint entanglement by admixing the $|e, g\rangle$ state. In Fig. 1(b), we show the concurrence \mathcal{C} of the steady state that follows from Eq. (12). For zero coupling, $\gamma = 0$, we get $\mathcal{C} = 0$, as the steady state is $|g, e\rangle$. However, as the coupling γ is turned on, entanglement is created and we observe a sweet spot [red in Fig. 1(b)] with a concurrence close to one, where the interfacial coupling is at around $\gamma \sim \sqrt{A(h_R - h_L)}$ and $\Delta \sim (h_L + h_R)/2$. As γ increases beyond the sweet spot, the pair creation appears more classical and entanglement only occurs in a narrow window around $\Delta = (h_L + h_R)/2$. At this tuned position we obtain $q_L = \bar{q}_R$ and the steady state becomes pure and has a particularly simple form given by Eq. (1). The concurrence in this case reduces to $\mathcal{C} = 2rt/(r^2 + t^2)$. We remark that the chiral nature of the coupling is not

essential to create entanglement. Without chirality, the spatial dependence of the scattering solution would survive [20].

Conclusion.—In this Letter, we demonstrated that steady-state entanglement can be imprinted onto a pair of color centers by letting them weakly interact with a magnetic solid-state environment. A necessary ingredient is to drive the environment out of equilibrium, which is achieved by an inverted magnet that can host negative-energy magnons (or antimagnons). At the interface to a normal magnet, positive-energy and negative-energy magnons are created in entangled pairs. Via a chiral magnetostatic coupling to the stray field of the magnet, the two color centers can pick up the magnon-antimagnon pairs through nonlocal absorption and emission processes. In a sweet spot, tuned by the color center energy and the interfacial exchange coupling, the color centers naturally evolve into an entangled steady state that even approaches the Bell state.

A key to imprinting entanglement was the creation of two-mode squeezing between positive-energy and negative-energy magnons. We emphasize that rather than an external drive, the interfacial exchange coupling served as an outlet that can harvest the energy supplied by the bulk inverted magnet. This is contrasted with the parametric drive used to create squeezing in quantum optics [18, 19, 27].

For future work, it might be interesting to embrace the full nonlinearity of the spin dynamics in the environment in order to prepare non-Gaussian states, going beyond two-mode squeezing. Furthermore, it seems promising to couple different magnetic systems to the inverted region that can be used as a source of energy to induce interesting entangled dynamics. Yet another promising route is to scale up the effect by considering two-dimensional generalizations, which allows an extended ensemble of color centers placed at interfaces between ground- and inverted-state regions.

This work was supported by the U.S. Department of Energy, Office of Basic Energy Sciences under Grant No. DE-SC0012190.

* ekleinherbers@physics.ucla.edu

- [1] A. Chatterjee, P. Stevenson, S. De Franceschi, A. Morello, N. P. de Leon, and F. Kuemmeth, Semiconductor qubits in practice, *Nature Reviews Physics* **3**, 157 (2021).
- [2] L. Trifunovic, O. Dial, M. Trif, J. R. Wootton, R. Abebe, A. Yacoby, and D. Loss, Long-distance spin-spin coupling via floating gates, *Phys. Rev. X* **2**, 011006 (2012).
- [3] M. W. Doherty, N. B. Manson, P. Delaney, F. Jelezko, J. Wrachtrup, and L. C. Hollenberg, The nitrogen-vacancy colour centre in diamond, *Physics Reports* **528**, 1 (2013).
- [4] R. Nagy, M. Niethammer, M. Widmann, Y.-C. Chen,

- P. Udvarhelyi, C. Bonato, J. U. Hassan, R. Karhu, I. G. Ivanov, N. T. Son, J. R. Maze, T. Ohshima, Ö. O. Soykal, Á. Gali, S.-Y. Lee, F. Kaiser, and J. Wrachtrup, High-fidelity spin and optical control of single silicon-vacancy centres in silicon carbide, *Nature Communications* **10**, 1954 (2019).
- [5] A. Gottscholl, M. Kianinia, V. Soltamov, S. Orlinskii, G. Mamin, C. Bradac, C. Kasper, K. Krambrock, A. Sperlich, M. Toth, I. Aharonovich, and V. Dyakonov, Initialization and read-out of intrinsic spin defects in a van der waals crystal at room temperature, *Nature Materials* **19**, 540 (2020).
- [6] G. Burkard, T. D. Ladd, A. Pan, J. M. Nichol, and J. R. Petta, Semiconductor spin qubits, *Rev. Mod. Phys.* **95**, 025003 (2023).
- [7] J. Zou, S. Zhang, and Y. Tserkovnyak, Bell-state generation for spin qubits via dissipative coupling, *Phys. Rev. B* **106**, L180406 (2022).
- [8] F. Casola, T. van der Sar, and A. Yacoby, Probing condensed matter physics with magnetometry based on nitrogen-vacancy centres in diamond, *Nature Reviews Materials* **3**, 17088 (2018).
- [9] A. Mzyk, A. Sigaeva, and R. Schirhagl, Relaxometry with nitrogen vacancy (nv) centers in diamond, *Accounts of Chemical Research* **55**, 3572 (2022).
- [10] G. Schaller, Quantum equilibration under constraints and transport balance, *Phys. Rev. E* **83**, 031111 (2011).
- [11] J. Harms, H. Yuan, and R. A. Duine, Enhanced magnon spin current using the bosonic klein paradox, *Phys. Rev. Appl.* **18**, 064026 (2022).
- [12] C. Mayoral, A. Fabbri, and M. Rinaldi, Steplike discontinuities in Bose-Einstein condensates and Hawking radiation: Dispersion effects, *Phys. Rev. D* **83**, 124047 (2011).
- [13] R. E. Wagner, M. R. Ware, Q. Su, and R. Grobe, Bosonic analog of the klein paradox, *Phys. Rev. A* **81**, 024101 (2010).
- [14] R. Balbinot, I. Carusotto, A. Fabbri, C. Mayoral, and A. Recati, Understanding hawking radiation from simple models of atomic bose-einstein condensates, in *Analogue Gravity Phenomenology: Analogue Spacetimes and Horizons, from Theory to Experiment*, edited by D. Faccio, F. Belgiorno, S. Cacciatori, V. Gorini, S. Liberati, and U. Moschella (Springer International Publishing, Cham, 2013) pp. 181–219.
- [15] A. Roldán-Molina, A. S. Nunez, and R. A. Duine, Magnonic black holes, *Phys. Rev. Lett.* **118**, 061301 (2017).
- [16] J. S. Harms, H. Y. Yuan, and R. A. Duine, Antimagnonics, *AIP Advances* **14**, 025303 (2024).
- [17] W. K. Wootters, Entanglement of formation of an arbitrary state of two qubits, *Phys. Rev. Lett.* **80**, 2245 (1998).
- [18] C. M. Caves and B. L. Schumaker, New formalism for two-photon quantum optics. i. quadrature phases and squeezed states, *Phys. Rev. A* **31**, 3068 (1985).
- [19] B. L. Schumaker and C. M. Caves, New formalism for two-photon quantum optics. ii. mathematical foundation and compact notation, *Phys. Rev. A* **31**, 3093 (1985).
- [20] See Supplemental Material at [URL will be inserted by publisher] for a detailed derivation of (i) the scattering solutions that are used to describe the magnon-antimagnon pair creation, (ii) the chiral magnetostatic coupling to the color centers.
- [21] G. B. Lesovik and I. A. Sadovskyy, Scattering matrix approach to the description of quantum electron transport, *Physics-Uspekhi* **54**, 1007 (2011).
- [22] A. L. Bassant, M. E. Y. Regout, J. S. Harms, and R. A. Duine, Entangled magnon-pair generation in a driven synthetic antiferromagnet, *Phys. Rev. B* **110**, 094441 (2024).
- [23] K. Y. Guslienko and A. N. Slavin, Magnetostatic Green's functions for the description of spin waves in finite rectangular magnetic dots and stripes, *J. Magn. Magn. Mater.* **323**, 2418 (2011).
- [24] K. Halbach, Application of permanent magnets in accelerators and electron storage rings, *Journal of Applied Physics* **57**, 3605 (1985).
- [25] B. Flebus and Y. Tserkovnyak, Quantum-impurity relaxometry of magnetization dynamics, *Phys. Rev. Lett.* **121**, 187204 (2018).
- [26] There is, however, a local Lamb shift $\propto \delta_\alpha \sigma_\alpha^z$ on either side, which renormalizes the bare energies Δ . The dynamics will be sensitive to differences $\delta_L - \delta_R$.
- [27] C. M. Caves, Quantum-mechanical noise in an interferometer, *Phys. Rev. D* **23**, 1693 (1981).

Entangling color centers via magnon-antimagnon pair creation

Eric Kleinherbers,^{*} Shane P. Kelly, and Yaroslav Tserkovnyak

*Department of Physics and Astronomy and Bhaumik Institute for Theoretical Physics,
University of California, Los Angeles, California 90095, USA*

(Dated: November 18, 2024)

CONTENTS

I. Notation	1
II. Magnon-antimagnon pair creation	1
A. Ground- and inverted-state ferromagnet	2
B. Exchange coupling at interface	3
C. Bogoliubov-de-Gennes space	4
D. Scattering solutions	4
1. Incoming magnon from the left	6
2. Incoming antimagnon from the right	7
3. Incoming magnon from the right	8
E. Magnon field operators	9
F. Spin current	9
G. Scattering matrix	9
H. Two-mode squeezing	10
III. Magnetic coupling to color centers	11
A. Stray magnetic field	11
B. Master equation	12
1. Dissipative coupling	12
2. Coherent coupling	13
C. Entanglement	14
IV. Exchange coupling to color centers	14
References	14

I. NOTATION

In the Letter, we introduced a more streamlined notation as we ignored unessential scattering solutions. In the Supplemental Material, our description is more complete and therefore uses a slightly different notation. The mapping between notations is given by

$$\begin{array}{c|c|c|c|c|c|c} \text{Letter} & a_\varepsilon & b_{-\varepsilon}^\dagger & r_a(\varepsilon) & t_a(-\varepsilon) & r_b(-\varepsilon) & t_b(\varepsilon) \\ \hline \text{Supplementary} & a_1(\varepsilon) & \bar{a}_2(\varepsilon) & r_1(\varepsilon) & \bar{t}_1(\varepsilon) & \bar{r}_2(\varepsilon) & t_2(\varepsilon) \end{array}$$

The expressions of the amplitudes can be read off from Eq. (33)-(34) and Eq. (38)-(39).

II. MAGNON-ANTIMAGNON PAIR CREATION

To describe the nonequilibrium environment, we use a generalized scattering theory in Bogoliubov space combining positive-energy and negative-energy magnonic excitations by using the language of antimagnonics [1]. We follow the calculations in close analogy to Ref. [2], where analog black holes in superfluids are studied. The full environment Hamiltonian can be decomposed as $H_E = \int dx (\mathcal{H}_L + \mathcal{H}_R + \mathcal{H}_I)$ which describes contributions of the left ground-state ferromagnet, the right inverted-state ferromagnet, and the coupling at the interface.

^{*} ekleinherbers@physics.ucla.edu

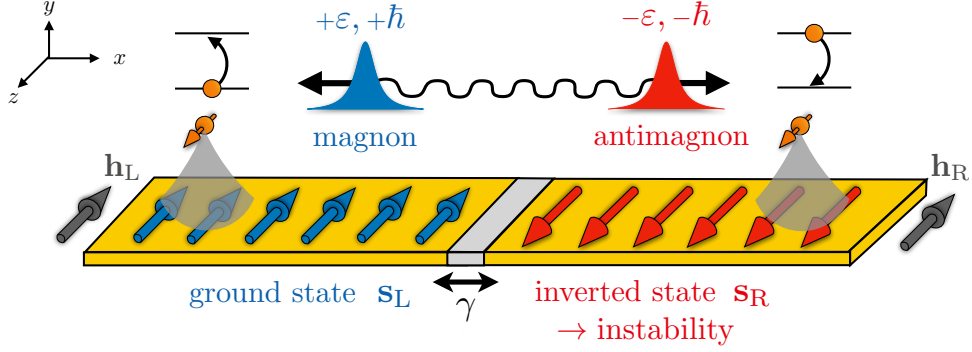


FIG. 1. Setup for pair creation of magnons (blue) and antimagnons (red) at an interface between two ferromagnets, one in the ground state (left) and one in an excited state (right). The latter is dynamically stabilized by spin transfer torques.

A. Ground- and inverted-state ferromagnet

We start with the bulk properties of the left and the right magnet. For this, we use an effective low-energy theory of the spin density \mathbf{s}_α , where the index $\alpha \in L, R$ labels the left and right magnet, respectively. The Hamiltonian density takes the form

$$\mathcal{H}_\alpha = \frac{\tilde{A}}{2} (\partial_x \mathbf{s}_\alpha)^2 - \mathbf{h}_\alpha \cdot \mathbf{s}_\alpha, \quad (1)$$

where \mathbf{s}_L and \mathbf{s}_R are only nonzero for $x < 0$ and $x > 0$, respectively. The first term describes the bulk exchange interaction with spin stiffness \tilde{A} that favors a parallel alignment of the spins. The second term describes the Zeeman energy, where we assume a stepwise magnetic field¹ $\mathbf{h}_L = -\tilde{h}_L \mathbf{e}_z$ for $x < 0$ and $\mathbf{h}_R = -\tilde{h}_R \mathbf{e}_z$ for $x > 0$ with $\tilde{h}_R > \tilde{h}_L > 0$. In the absence of \mathcal{H}_I , the ferromagnet is aligned with \mathbf{h}_L on the left side and, thus, in its ground state with $\langle \mathbf{s}_L \rangle = -s \mathbf{e}_z$, where s is the spin density per length. On the right, on the other hand, the ferromagnet is antialigned with \mathbf{h}_R which we refer to as the *inverted state* with $\langle \mathbf{s}_R \rangle = +s \mathbf{e}_z$. The equations of motion follow from Heisenberg equations and are given by

$$\partial_t \mathbf{s}_L = \mathbf{s}_L \times \left(\tilde{A} \partial_x^2 \mathbf{s}_L + \mathbf{h}_L \right) - \frac{\alpha}{s} \mathbf{s}_L \times \partial_t \mathbf{s}_L, \quad \text{for } x < 0, \quad (2)$$

$$\partial_t \mathbf{s}_R = \mathbf{s}_R \times \left(\tilde{A} \partial_x^2 \mathbf{s}_R + \mathbf{h}_R \right) - \frac{\alpha}{s} \mathbf{s}_R \times \partial_t \mathbf{s}_R + \frac{\tau_S}{s} \mathbf{s}_R \times (\mathbf{s}_R \times \mathbf{e}_z), \quad \text{for } x > 0, \quad (3)$$

where we used the spin commutation relations $[s_i(x), s_j(x')] = 2\hbar \varepsilon_{ijk} s_k(x) \delta(x-x')$. In addition, we added dissipation via Gilbert damping with damping factor α and a spin torque described by τ_S to drive the system.

For a linearized treatment of spin excitations, we use the usual Holstein-Primakoff bosonic fields in the large spin limit

$$\psi_L = \frac{1}{\sqrt{2\hbar s}} (s_L^x - i s_L^y), \quad (4)$$

$$\psi_R = \frac{1}{\sqrt{2\hbar s}} (s_R^x + i s_R^y), \quad (5)$$

which describe magnonic excitations with spin $+\hbar$ and $-\hbar$ on top of the ground and the inverted state, respectively. They obey the bosonic commutation relations $[\psi_{L,R}(x), \psi_{L,R}^\dagger(x')] = \delta(x-x')$. The Hamiltonian becomes bilinear after normal ordering and we obtain

$$\mathcal{H}_\alpha = A (\partial_x \psi_\alpha^\dagger) (\partial_x \psi_\alpha) \pm h_\alpha \psi_\alpha^\dagger \psi_\alpha, \quad (6)$$

¹ Here, we define the field $\mathbf{h}_{L,R}$ as the actual magnetic field times the gyromagnetic ratio $\gamma_e = g_e \mu_B / \hbar < 0$ with the g-factor $g_e \approx -2$ and the Bohr magneton μ_B . Then, the energy is minimized when the spin density $\mathbf{s}_{L,R}$ and the field $\mathbf{h}_{L,R}$ point in the same direction.

where the positive (negative) sign holds for the left (right) magnet. Here, we defined a rescaled spin stiffness $A = \hbar s \tilde{A}/2$ and magnetic field $h_\alpha = \hbar \tilde{h}_\alpha$. The bulk field equations become

$$i\hbar\partial_t\psi_L = (1 - i\alpha)(-A\partial_x^2 + h_L)\psi_L, \quad \text{for } x < 0, \quad (7)$$

$$i\hbar\partial_t\psi_R = (1 - i\alpha)(-A\partial_x^2 - h_R)\psi_R + i\hbar\tau_S\psi_R, \quad \text{for } x > 0. \quad (8)$$

The associated bulk excitation energies of the magnons are given by $\varepsilon_{L,R} = Ak^2 \pm h_{L,R}$ (blue) for the left and right magnets which are shown in Fig. 2(a) and Fig. 2(b) as a function of the wavenumber k , respectively. The magnon energies are increased by h_L in the left magnet, while they are lowered by h_R in the right magnet. As a result, we obtain negative excitation energies, $\varepsilon_R < 0$, which indicates the instability of the inverted magnet. Due to Gilbert damping the magnon excitation energies acquire an imaginary part, $-i\alpha\varepsilon$. For positive energies, $\varepsilon_{L,R} > 0$, this leads to an exponential decay of the magnon mode. However, for negative energies, $\varepsilon_{L,R} < 0$, the magnon modes grow exponentially and eventually flip the whole magnet to its ground state. Here, we want to avoid this growing instability by dynamically stabilizing the system with a spin torque described by τ_S that effectively suppresses all magnon excitations and leaves the system in the inverted vacuum state. Specifically, if $-\hbar\tau_S > \alpha h_R$, the system will be dynamically stable.

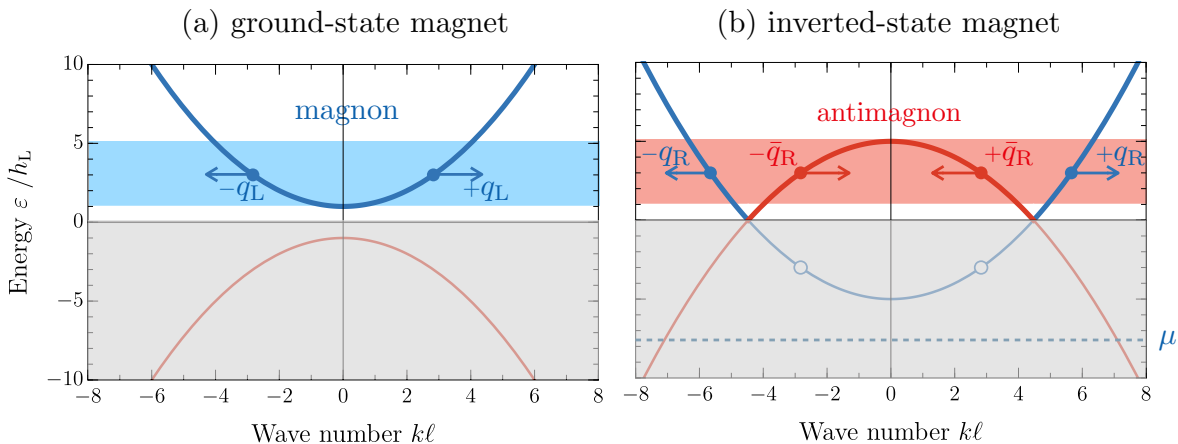


FIG. 2. Magnon excitation energies $\varepsilon_{L,R}$ (blue lines) for (a) the left and (b) the right magnet. The right magnet is in an unstable inverted state, which gives rise to negative excitation energies, $\varepsilon_R < 0$. Formally, we can add the antimagnonic excitation energies $\bar{\varepsilon}_{L,R}$ (red lines) with an inverted sign and disregard all negative energies (gray area). For energies $h_L < \varepsilon_L < h_R$ (blue area on the left) and $h_L < \bar{\varepsilon}_R < h_R$ (red area on the right) magnons and antimagnons can be created pairwise at the interface. We choose $h_R = 5h_L$ and we define the length scale $\ell = \sqrt{A/(h_R - h_L)}$.

B. Exchange coupling at interface

At the interface, both magnets are coupled via exchange interaction

$$\mathcal{H}_I = \tilde{\gamma}\delta(x)\mathbf{s}_L \cdot \mathbf{s}_R = \gamma\delta(x)\left(\psi_L^\dagger\psi_L + \psi_R^\dagger\psi_R + \psi_L\psi_R + \psi_L^\dagger\psi_R^\dagger\right), \quad (9)$$

where we, again, rescale the coupling parameter through $\gamma = \hbar s \tilde{\gamma}$. The sign of γ can be either ferromagnetic or antiferromagnetic. Crucially, this coupling contains terms of the form $\sim \delta(x)\psi_L^\dagger\psi_R^\dagger$ which become resonant when positive-energy magnons in the left magnet [blue filled dots in Fig. 2(a)] are matched with negative-energy magnons (or antimagnons) in the right magnet [blue empty dots in Fig. 2(b)]. This can only happen for energies in the interval $h_L < \varepsilon_L < h_R$ (indicated by the blue area). In this way, the interfacial coupling serves as a controlled outlet to harvest

the instability by creating entangled pairs of magnons.² The exchange coupling modifies the equations of motion to

$$i\hbar\partial_t\psi_L = [-A\partial_x^2 + h_L]\psi_L + \gamma\delta(x)\left(\psi_L + \psi_R^\dagger\right), \quad (10)$$

$$i\hbar\partial_t\psi_R = [-A\partial_x^2 - h_R]\psi_R + \gamma\delta(x)\left(\psi_R + \psi_L^\dagger\right), \quad (11)$$

where we neglect dissipation and driving in the following. Note that creation and annihilation operators are coupled at the interface. Therefore, in the next section, we will extend the formalism to the bosonic Bogoliubov-de-Gennes space.

C. Bogoliubov-de-Gennes space

To account for the magnon pair creation, we rewrite the field equations in a bosonic Bogoliubov-de-Gennes space

$$i\hbar\partial_t \begin{pmatrix} \psi_L \\ \psi_L^\dagger \end{pmatrix} = \mathcal{H}_L^{\text{BdG}} \begin{pmatrix} \psi_L \\ \psi_L^\dagger \end{pmatrix}, \quad \text{for } x < 0, \quad (12)$$

$$i\hbar\partial_t \begin{pmatrix} \psi_R \\ \psi_R^\dagger \end{pmatrix} = \mathcal{H}_R^{\text{BdG}} \begin{pmatrix} \psi_R \\ \psi_R^\dagger \end{pmatrix}, \quad \text{for } x > 0. \quad (13)$$

Here, we defined the effective bosonic Bogoliubov-de-Gennes Hamiltonian $\mathcal{H}_{L,R}^{\text{BdG}} = (-A\partial_x^2 \pm h_{L,R})\tau_z$, where τ_x , τ_y , and τ_z are the Pauli matrices. The corresponding bulk eigenvalues are given by

$$\varepsilon_{L,R} = Ak^2 \pm h_{L,R}, \quad \bar{\varepsilon}_{L,R} = -Ak^2 \mp h_{L,R}, \quad (14)$$

which are both shown in Fig. 2 in blue and red, respectively. Since we effectively introduced a redundancy by doubling the degrees of freedom, positive- and negative-energy solutions are related to each other through [1]

$$\tau_x \mathcal{H}_\alpha^{\text{BdG}} \tau_x = -(\mathcal{H}_\alpha^{\text{BdG}})^*. \quad (15)$$

Therefore, in the enlarged Bogoliubov-de-Gennes space, we can disregard all negative energies (gray area in Fig. 2) and only consider $\varepsilon > 0$. For the instability on the right side, $\varepsilon_R < 0$, this means that negative-energy magnons (or antimagnons) will be described by the inverted (or antimagnonic) branch $\bar{\varepsilon}_R$.

We remark that even though the Hamiltonians $\mathcal{H}_\alpha^{\text{BdG}}$ are hermitian, hermiticity will not be guaranteed for more generic systems when for example a magnetic anisotropy is included. However, the Hamiltonian will always obey pseudo hermiticity, $\tau_z \mathcal{H}_\alpha^{\text{BdG}} \tau_z = (\mathcal{H}_\alpha^{\text{BdG}})^\dagger$, as the evolution generated by $\mathcal{H}_\alpha^{\text{BdG}}$ conserves the commutation relations of ψ_α and ψ_α^\dagger .

D. Scattering solutions

Our goal is to find the magnon field operator $\psi_\alpha(x, t)$ expanded in the scattering solutions of the problem. It can be written using the Bogoliubov ansatz [1, 2]

$$\psi_\alpha(x, t) = \int_0^\infty d\varepsilon \sum_i \left[e^{-i\varepsilon t/\hbar} u_i(\varepsilon, x) a_i(\varepsilon) + e^{i\varepsilon t/\hbar} v_i^*(\varepsilon, x) a_i^\dagger(\varepsilon) \right], \quad (16)$$

where u_i and v_i correspond to the normal and anomalous amplitudes of the scattering solutions, respectively.³ Here, the operators a_i describe the in-scattering eigenstates (defined below) at a given energy ε and hence diagonalize the scattering problem. They fulfill the commutation relations

$$[a_i(\varepsilon), a_j^\dagger(\varepsilon')] = \Sigma_{ij} \delta(\varepsilon - \varepsilon'), \quad (17)$$

² We remark a formal similarity to a parametric drive often used in quantum optics to create squeezed states. Here, however, \mathcal{H}_C is not a drive but an energy-conserving coupling Hamiltonian that merely connects the stable and inverted region with each other and, thereby, enables the pair creation. Here, the instability is dissipatively stabilized.

³ W

where the diagonal signature matrix is given by $\Sigma_{ij} = \nu_i \delta_{ij}$. Due to the restriction to positive energies, $\varepsilon > 0$, we obtain two kinds of in-scattering solutions with $\nu_i = \pm 1$. The sign is determined by the character of the incoming state. For an incoming positive-energy magnon, we get $\nu_i = +1$, and the operator $a_i(\varepsilon)$ functions as an annihilation operator. For an incoming negative-energy magnon (or antimagnon), we get $\nu_i = -1$, and the operator $a_i(\varepsilon) = b_i^\dagger(-\varepsilon)$ functions as a creation operator. Formally, the sign is determined by the normalization of the scattering modes [2]:

$$\int dx [u_i^*(\varepsilon, x)u_j(\varepsilon', x) - v_i(\varepsilon, x)v_j^*(\varepsilon', x)] = \nu_i \delta_{ij} \delta(\varepsilon - \varepsilon'). \quad (18)$$

To derive the specific form of the scattering states, we insert Eq. (16) into Eq. (12)-(13) and apply the commutator from Eq. (17) to obtain the equations

$$\varepsilon \begin{pmatrix} u_{L,i} \\ v_{L,i} \end{pmatrix} = \mathcal{H}_L^{\text{BdG}} \begin{pmatrix} u_{L,i} \\ v_{L,i} \end{pmatrix}, \quad \text{for } x < 0, \quad (19)$$

$$\varepsilon \begin{pmatrix} u_{R,i} \\ v_{R,i} \end{pmatrix} = \mathcal{H}_R^{\text{BdG}} \begin{pmatrix} u_{R,i} \\ v_{R,i} \end{pmatrix}, \quad \text{for } x > 0, \quad (20)$$

where we introduce the indices L and R in the amplitudes u_i and v_i to indicate $x < 0$ and $x > 0$, respectively. In addition, the coupling at the interface leads to the boundary conditions

$$\left(\partial_x + \frac{\gamma}{A}\right) \begin{pmatrix} u_{L,i} \\ v_{L,i} \end{pmatrix} = -\frac{\gamma}{A} \tau_x \begin{pmatrix} u_{R,i} \\ v_{R,i} \end{pmatrix}, \quad \text{for } x = 0, \quad (21)$$

$$\left(\partial_x - \frac{\gamma}{A}\right) \begin{pmatrix} u_{R,i} \\ v_{R,i} \end{pmatrix} = +\frac{\gamma}{A} \tau_x \begin{pmatrix} u_{L,i} \\ v_{L,i} \end{pmatrix}, \quad \text{for } x = 0, \quad (22)$$

which can be obtained by integrating Eq. (10)-(11) over a small interval around the interface $x = 0$. Thus, at the interface, we only couple normal modes on the left ($u_{L,i}$) with anomalous modes on the right ($v_{R,i}$) and vice versa. To find the scattering solutions, we make a piecewise expansion in terms of the four eigenmodes of the bulk equations Eq. (19)-(20). The scattering states will then be a superposition of the following bulk eigenmodes

$$m_{\alpha,\pm} = \frac{1}{\sqrt{2\pi\hbar v_\alpha}} e^{\pm i q_\alpha x} \begin{pmatrix} 1 \\ 0 \end{pmatrix}, \quad \bar{m}_{\alpha,\pm} = \frac{1}{\sqrt{2\pi\hbar \bar{v}_\alpha}} e^{\mp i \bar{q}_\alpha x} \begin{pmatrix} 0 \\ 1 \end{pmatrix}, \quad (23)$$

where the first term describes pure right-moving ($m_{\alpha,+}$) and left-moving ($m_{\alpha,-}$) magnons and the second term describes pure right-moving ($\bar{m}_{\alpha,+}$) and left-moving ($\bar{m}_{\alpha,-}$) antimagnons. Since the spin z angular momentum is conserved, the eigenmodes do not mix normal and anomalous amplitudes. The wave numbers and absolute group velocities are denoted by q_α and v_α for magnons and \bar{q}_α and \bar{v}_α for antimagnons, respectively. Note that for antimagnons, we introduced a relative sign change in the exponent since momentum and group velocity are of opposite sign. The wave numbers in the left magnet can be derived from Eq. (19) and are given by

$$q_L = \frac{1}{\sqrt{A}} \begin{cases} \sqrt{\varepsilon - h_L}, & \text{for } \varepsilon \geq h_L \\ i\sqrt{h_L - \varepsilon}, & \text{for } \varepsilon \leq h_L \end{cases} \quad \text{and} \quad \bar{q}_L = -i \frac{\sqrt{\varepsilon + h_L}}{\sqrt{A}}. \quad (24)$$

The wave numbers in the right magnet are derived from Eq. (20) and are given by

$$q_R = \frac{\sqrt{\varepsilon + h_R}}{\sqrt{A}} \quad \text{and} \quad \bar{q}_R = \frac{1}{\sqrt{A}} \begin{cases} -i\sqrt{\varepsilon - h_R}, & \text{for } \varepsilon \geq h_R \\ \sqrt{h_R - \varepsilon}, & \text{for } \varepsilon \leq h_R \end{cases}. \quad (25)$$

We choose the signs of the imaginary wavenumbers such that the derived results below do not contain exponentially growing solutions. The absolute values of the group velocities are given by

$$v_\alpha = \frac{2A|q_L|}{\hbar}, \quad \bar{v}_\alpha = \frac{2A|\bar{q}_L|}{\hbar}, \quad (26)$$

which are only meaningful for propagating modes. However, to keep the notation uniform, we also define them for the evanescent modes. They are included in Eq. (23) to ensure a proper normalization in the energy eigenbasis⁴. Now, a

⁴ By including the group velocity, the propagating eigenmodes are normalized on delta functions in energy, $\int dx \frac{1}{\sqrt{2\pi\hbar v_\alpha(\varepsilon)}} e^{+iq_\alpha(\varepsilon)x} \frac{1}{\sqrt{2\pi\hbar v_\alpha(\varepsilon')}} e^{-iq_\alpha(\varepsilon')x} = \delta(\varepsilon - \varepsilon')$.

general scattering solution can be expanded in terms of $m_{\alpha,\pm}$ and $\bar{m}_{\alpha,\pm}$ and we use the ansatz

$$\begin{pmatrix} u_{\alpha,i} \\ v_{\alpha,i} \end{pmatrix} = a_{\alpha,i} m_{\alpha,+} + b_{\alpha,i} m_{\alpha,-} + \bar{a}_{\alpha,i} \bar{m}_{\alpha,+} + \bar{b}_{\alpha,i} \bar{m}_{\alpha,-}, \quad (27)$$

where $a_{\alpha,i}$ and $\bar{a}_{\alpha,i}$ ($b_{\alpha,i}$ and $\bar{b}_{\alpha,i}$) are the energy-dependent amplitudes of the right-moving (left-moving) magnon and antimagnon modes, respectively. The amplitudes are determined through the boundary conditions which can be rewritten as

$$\mathcal{W}_L \mathcal{N}_L \begin{pmatrix} a_{L,i} \\ b_{L,i} \\ \bar{a}_{L,i} \\ \bar{b}_{L,i} \end{pmatrix} = \mathcal{W}_R \mathcal{N}_R \begin{pmatrix} a_{R,i} \\ b_{R,i} \\ \bar{a}_{R,i} \\ \bar{b}_{R,i} \end{pmatrix}, \quad (28)$$

where we introduced the diagonal normalization matrices $\mathcal{N}_\alpha = \sqrt{2\pi \text{diag}(v_\alpha, v_\alpha, \bar{v}_\alpha, \bar{v}_\alpha)}^{-1}$ as well as the matrices

$$\mathcal{W}_L = \begin{pmatrix} iq_L + \frac{\gamma}{A} & -iq_L + \frac{\gamma}{A} & 0 & 0 \\ 0 & 0 & -i\bar{q}_L + \frac{\gamma}{A} & i\bar{q}_L + \frac{\gamma}{A} \\ \frac{\gamma}{A} & \frac{\gamma}{A} & 0 & 0 \\ 0 & 0 & \frac{\gamma}{A} & \frac{\gamma}{A} \end{pmatrix}, \quad \mathcal{W}_R = \begin{pmatrix} 0 & 0 & -\frac{\gamma}{A} & -\frac{\gamma}{A} \\ -\frac{\gamma}{A} & -\frac{\gamma}{A} & 0 & 0 \\ 0 & 0 & -i\bar{q}_R - \frac{\gamma}{A} & +i\bar{q}_R - \frac{\gamma}{A} \\ iq_R - \frac{\gamma}{A} & -iq_R - \frac{\gamma}{A} & 0 & 0 \end{pmatrix}, \quad (29)$$

which directly follow from Eq. (21)-(22) and Eq. (27). By defining the transfer matrix $\mathcal{M} = (\mathcal{W}_L \mathcal{N}_L)^{-1} \mathcal{W}_R \mathcal{N}_R$, we can relate the solutions on the left and right side of the interface via

$$\begin{pmatrix} a_{L,i} \\ b_{L,i} \\ \bar{a}_{L,i} \\ \bar{b}_{L,i} \end{pmatrix} = \mathcal{M} \begin{pmatrix} a_{R,i} \\ b_{R,i} \\ \bar{a}_{R,i} \\ \bar{b}_{R,i} \end{pmatrix}. \quad (30)$$

In the following, we will consider all three scattering solutions in the interval $h_L < \varepsilon < h_R$. However, the results are written such that they are correct for all energies.

1. Incoming magnon from the left

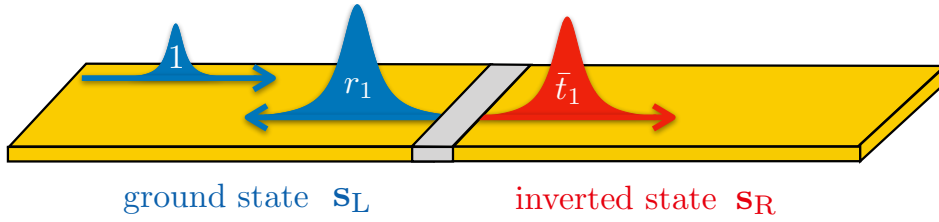


FIG. 3. Schematics of the in-scattering solution a_1 . An incoming magnon with amplitude 1 is reflected with an enhanced amplitude $|r_1| > 1$ and transmitted as an antimagnon with \bar{t}_1 . The relative size of the wave packages schematically indicates that $|r_1|^2 - |\bar{t}_1|^2 = 1$.

To find the first in-scattering solution with magnonic operator a_1 , we assume for the scattering boundary condition an incoming magnon mode from the left. We use the ansatz

$$\begin{pmatrix} a_{L,1} \\ b_{L,1} \\ \bar{a}_{L,1} \\ \bar{b}_{L,1} \end{pmatrix} = \begin{pmatrix} i_1 \\ r_1 \\ 0 \\ \bar{r}_1 \end{pmatrix}, \quad \begin{pmatrix} a_{R,1} \\ b_{R,1} \\ \bar{a}_{R,1} \\ \bar{b}_{R,1} \end{pmatrix} = \begin{pmatrix} t_1 \\ 0 \\ \bar{t}_1 \\ 0 \end{pmatrix}. \quad (31)$$

There is an incoming right-moving magnon from the left with amplitude

$$i_1 = \Theta(\varepsilon - h_L) \quad (32)$$

that can be reflected back as a propagating magnon with amplitude r_1 or as an evanescent antimagnon with amplitude \bar{r}_1 . On the right side, the magnon can be transmitted with amplitudes t_1 and \bar{t}_1 as a magnon and antimagnon, respectively. The remaining amplitudes are zero because no other propagating modes are incoming, and we disregard exponentially growing solutions. With Eq. (30), we find for the magnonic reflection amplitude

$$r_1 = \Theta(\varepsilon - h_L) \frac{q_L \bar{q}_R - i \frac{\gamma}{A} (q_L + \bar{q}_R)}{q_L \bar{q}_R - i \frac{\gamma}{A} (q_L - \bar{q}_R)}, \quad (33)$$

and for the antimagnonic transmission amplitude

$$\bar{t}_1 = \Theta(\varepsilon - h_L) \frac{-2 \frac{\gamma}{A} q_L}{i q_L \bar{q}_R + \frac{\gamma}{A} (q_L - \bar{q}_R)} \sqrt{\left| \frac{\bar{q}_R}{q_L} \right|}. \quad (34)$$

The remaining amplitudes are zero, $\bar{r}_1 = t_1 = 0$, because the spin z angular momentum is conserved. Hence, the magnon can neither be reflected as an antimagnon nor can it be transmitted as a magnon. Note that

$$|r_1|^2 - |\bar{t}_1|^2 = 1 \quad \text{for} \quad h_L < \varepsilon < h_R. \quad (35)$$

The reflection of magnons is effectively enhanced, $|r_1|^2 \geq 1$, which is already a hint at the underlying pair creation of magnons and antimagnons at the interface.

2. Incoming antimagnon from the right

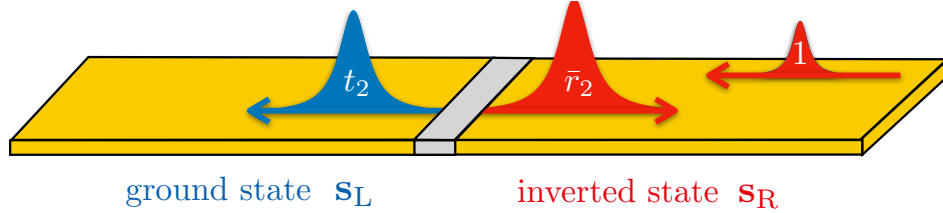


FIG. 4. Schematics of the in-scattering solution a_2 . An incoming antimagnon with amplitude 1 is reflected with an enhanced amplitude $|\bar{r}_2| > 1$ and transmitted as a magnon with t_2 . The relative size of the wave packages schematically indicates that $|\bar{r}_2|^2 - |t_2|^2 = 1$.

To find the second in-scattering solution with antimagnonic operator a_2 , we assume for the scattering boundary condition an incoming antimagnon from the right. We use the ansatz

$$\begin{pmatrix} a_{L,2} \\ b_{L,2} \\ \bar{a}_{L,2} \\ \bar{b}_{L,2} \end{pmatrix} = \begin{pmatrix} 0 \\ t_2 \\ 0 \\ \bar{t}_2 \end{pmatrix}, \quad \begin{pmatrix} a_{R,2} \\ b_{R,2} \\ \bar{a}_{R,2} \\ \bar{b}_{R,2} \end{pmatrix} = \begin{pmatrix} r_2 \\ 0 \\ \bar{r}_2 \\ \bar{i}_2 \end{pmatrix}. \quad (36)$$

The incoming left-moving antimagnon from the right with amplitude

$$\bar{i}_2 = \Theta(h_R - \varepsilon) \quad (37)$$

can be reflected back as a magnon or antimagnon with amplitude r_2 and \bar{r}_2 , respectively. On the left side, the antimagnon can be transmitted either as a propagating magnon with amplitude t_2 or as an evanescent antimagnon with amplitude \bar{t}_2 . The remaining amplitudes are zero because no other propagating modes are incoming, and we disregard exponentially growing solutions. With Eq. (30), we find for the antimagnonic reflection amplitude

$$\bar{r}_2 = \Theta(h_R - \varepsilon) \frac{q_L \bar{q}_R + i \frac{\gamma}{A} (q_L + \bar{q}_R)}{q_L \bar{q}_R - i \frac{\gamma}{A} (q_L - \bar{q}_R)}, \quad (38)$$

and for the magnonic transmission amplitude

$$t_2 = \Theta(h_R - \varepsilon) \frac{2 \frac{\gamma}{A} \bar{q}_R}{i q_L \bar{q}_R + \frac{\gamma}{A} (q_L - \bar{q}_R)} \sqrt{\left| \frac{q_L}{\bar{q}_R} \right|}. \quad (39)$$

The remaining amplitudes are zero, $r_2 = \bar{t}_2 = 0$, because the spin z angular momentum is conserved. Hence, the antimagnon can neither be reflected as a magnon nor can it be transmitted as an antimagnon. Note that

$$|\bar{r}_2|^2 - |t_2|^2 = 1 \quad \text{for } h_L < \varepsilon < h_R. \quad (40)$$

The reflection of antimagnons is effectively enhanced, $|r_1|^2 \geq 1$, which is already a hint at the underlying pair creation of magnons and antimagnons at the interface.

3. Incoming magnon from the right

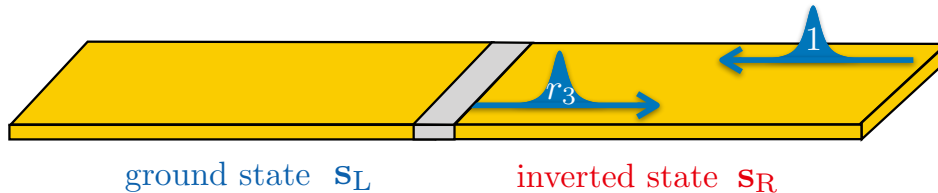


FIG. 5. Schematics of the in-scattering solution a_3 . An incoming magnon with amplitude 1 is fully reflected with amplitude $|r_3| = 1$ and there is no transmission (only evanescent modes).

To find the third in-scattering solution with magnonic operator a_3 , we assume for the scattering boundary condition an incoming magnon mode from the right. We use the ansatz

$$\begin{pmatrix} a_{L,3} \\ b_{L,3} \\ \bar{a}_{L,3} \\ \bar{b}_{L,3} \end{pmatrix} = \begin{pmatrix} 0 \\ t_3 \\ 0 \\ \bar{t}_3 \end{pmatrix}, \quad \begin{pmatrix} a_{R,3} \\ b_{R,3} \\ \bar{a}_{R,3} \\ \bar{b}_{R,3} \end{pmatrix} = \begin{pmatrix} r_3 \\ i_3 \\ \bar{r}_3 \\ 0 \end{pmatrix}. \quad (41)$$

There is an incoming left-moving magnon from the right with amplitude

$$i_3 = 1, \quad (42)$$

which can be reflected back as a magnon or antimagnon with amplitude r_3 and \bar{r}_3 , respectively. On the left side, the antimagnon can be transmitted as a propagating magnon with amplitude t_3 or as an evanescent antimagnon with amplitude \bar{t}_3 . The remaining amplitudes are zero because no other propagating modes are incoming, and we disregard exponentially growing solutions. With Eq. (30), we find for the magnonic reflection amplitude

$$r_3 = \frac{\bar{q}_L q_R - i \frac{\gamma}{A} (\bar{q}_L + q_R)}{\bar{q}_L q_R + i \frac{\gamma}{A} (\bar{q}_L - q_R)}, \quad (43)$$

and for the evanescent antimagnonic amplitude on the left side

$$\bar{t}_3 = \frac{-2 \frac{\gamma}{A} \sqrt{\bar{q}_L q_R}}{i \bar{q}_L q_R - \frac{\gamma}{A} (\bar{q}_L - q_R)}. \quad (44)$$

The remaining amplitudes are zero, $\bar{r}_3 = t_3 = 0$, because the spin z angular momentum is conserved. Hence, the magnon can neither be reflected as an antimagnon nor can it be transmitted as a magnon. Note that $|r_3|^2 = 1$, i.e., the magnon is fully reflected.

E. Magnon field operators

Inserting the scattering solutions into the magnon field operators, we finally get

$$\psi_L(x, t) = \int_0^\infty \frac{d\varepsilon}{\sqrt{2\pi\hbar v_L}} \left[(i_1 e^{iq_L x} + r_1 e^{-iq_L x}) e^{-i\varepsilon t/\hbar} a_1 + t_2 e^{-iq_L x} e^{-i\varepsilon t/\hbar} a_2 + \sqrt{\frac{v_L}{\bar{v}_L}} (t_3 e^{i\bar{q}_L x})^* e^{i\varepsilon t/\hbar} a_3^\dagger \right], \quad (45)$$

$$\psi_R^\dagger(x, t) = \int_0^\infty \frac{d\varepsilon}{\sqrt{2\pi\hbar v_R}} \left[(\bar{t}_1 e^{-i\bar{q}_R x}) e^{-i\varepsilon t/\hbar} a_1 + (\bar{i}_2 e^{i\bar{q}_R x} + \bar{r}_2 e^{-i\bar{q}_R x}) e^{-i\varepsilon t/\hbar} a_2 + \sqrt{\frac{\bar{v}_R}{v_R}} (i_3 e^{-iq_R x} + r_3 e^{iq_R x})^* e^{i\varepsilon t/\hbar} a_3^\dagger \right], \quad (46)$$

where the first (second) line holds for $x < 0$ ($x > 0$). In the following, we will be interested in the vacuum state $|\Omega\rangle$, where no magnon or antimagnon is incoming from the boundary. It can be defined through

$$a_1 |\Omega\rangle = a_2^\dagger |\Omega\rangle = a_3 |\Omega\rangle = 0, \quad (47)$$

for each energy ε . Note that for the antimagnonic mode, we have $a_2(\varepsilon) = b_2^\dagger(-\varepsilon)$. Thus, it effectively corresponds to the creation operator of a negative-energy magnon.

F. Spin current

The spin current is given by

$$I_\alpha^s = - : \tilde{A} \mathbf{e}_z \cdot (\mathbf{s}_\alpha \times \partial_x \mathbf{s}_\alpha) :, \quad (48)$$

where we use normal ordering in ψ_α and ψ_α^\dagger . It results into

$$\hat{I}_L^s = +2A \left[\psi_L^\dagger (-i\partial_x \psi_L) - (-i\partial_x \psi_L^\dagger) \psi_L \right], \quad \text{for } x < 0, \quad (49)$$

$$\hat{I}_R^s = -2A \left[\psi_R^\dagger (-i\partial_x \psi_R) - (-i\partial_x \psi_R^\dagger) \psi_R \right], \quad \text{for } x > 0. \quad (50)$$

In the vacuum $|\Omega\rangle$, we get

$$\langle \Omega | \hat{I}_L^s(x) | \Omega \rangle = -\frac{2\hbar}{h} \int_{h_L}^{h_R} d\varepsilon |t_2(\varepsilon)|^2, \quad (51)$$

$$\langle \Omega | \hat{I}_R^s(x) | \Omega \rangle = -\frac{2\hbar}{h} \int_{h_L}^{h_R} d\varepsilon |\bar{t}_1(\varepsilon)|^2, \quad (52)$$

where we write the proportionality constant in analogy to the electron current in the Landauer-Büttiker formalism [3], where we get $\frac{2e}{h}$ with $h = 2\pi\hbar$. Thus, the system sustains a spin current that is moving to the left. This current is purely quantum as it originates in the vacuum fluctuations at the interface. It manifests itself as a constant creation of magnon-antimagnon pairs, where $+\hbar$ magnons move into the left magnet and $-\hbar$ antimagnons move into the right magnet. The spin current is the same for all x since $|\bar{t}_1| = |t_2| = t$. We can also define the spin current per energy via $j^s(\varepsilon) = t^2/\pi$.

G. Scattering matrix

Instead of expanding the field operators in the basis of in-scattering eigenstates $u_{\alpha,i}^{\text{in}}$ and $v_{\alpha,i}^{\text{in}}$, which we derived above, we can also choose their time-inverted partners, the out-scattering states $u_{\alpha,i}^{\text{out}} = (u_{\alpha,i}^{\text{in}})^*$ and $v_{\alpha,i}^{\text{out}} = (v_{\alpha,i}^{\text{in}})^*$, which are related to the former by complex conjugation. Since both of them form a proper basis, the in- and out-scattering states can be linearly related to each other for each energy ε via

$$u_{\alpha,i}^{\text{in}} = \sum_j (S^T)_{ij} u_{\alpha,j}^{\text{out}}, \quad v_{\alpha,i}^{\text{in}} = \sum_j (S^T)_{ij} v_{\alpha,j}^{\text{out}}, \quad (53)$$

where the matrix S^T is the transpose of the scattering matrix S and does not depend on α . Now, we can insert this relation into the field operator expansion Eq. (16) and make use of the rearrangement

$$\sum_i u_{\alpha,i}^{\text{in}} a_i^{\text{in}} = \sum_{i,j} (S^T)_{ij} u_{\alpha,j}^{\text{out}} a_i^{\text{in}} = \sum_i u_{\alpha,i}^{\text{out}} \sum_j S_{ij} a_j^{\text{in}} = \sum_i u_{\alpha,i}^{\text{out}} a_i^{\text{out}}. \quad (54)$$

The same rearrangement can be done for the terms involving $v_{\alpha,i}^{\text{in}}$. This way, we define the annihilation operators for out-scattering states by $a_i^{\text{out}} = \sum_j S_{ij} a_j^{\text{in}}$. For $h_L < \varepsilon < h_R$, we get

$$\begin{pmatrix} a_1^{\text{out}} \\ a_2^{\text{out}} \\ a_3^{\text{out}} \end{pmatrix}_{\text{out}} = \underbrace{\begin{pmatrix} r_1 & t_2 & 0 \\ \bar{t}_1 & \bar{r}_2 & 0 \\ 0 & 0 & r_3 \end{pmatrix}}_S \begin{pmatrix} a_1^{\text{in}} \\ a_2^{\text{in}} \\ a_3^{\text{in}} \end{pmatrix}. \quad (55)$$

To find the scattering matrix we used Eq. (53). From the time reversal relation between in- and out-scattering states, it follows that

$$S^* S = \mathbf{1}. \quad (56)$$

Moreover, the scattering matrix S conserves the magnonic and antimagnonic commutation relations such that

$$S \Sigma S^\dagger = \Sigma, \quad (57)$$

where $\Sigma = \text{diag}(1, -1, 1)$. Thus, magnons are mapped to magnons and antimagnons to antimagnons. Combining both relations yields $t_2 = -\bar{t}_1$ and $t_2^* \bar{r}_2 = \bar{t}_1 r_1^*$ as well as

$$|r_1|^2 - |\bar{t}_1|^2 = 1 \quad \text{and} \quad |\bar{r}_2|^2 - |t_2|^2 = 1. \quad (58)$$

H. Two-mode squeezing

Alternatively, the relation between $a_{1,2}^{\text{in}}$ and $a_{1,2}^{\text{out}}$ from Eq. (55) can also be formulated in Fock space using a two-mode squeezing transformation U such that

$$e^{-i\phi_1} a_1^{\text{out}} = U^\dagger a_1^{\text{in}} U = \cosh r a_1^{\text{in}} - e^{+i\theta} \sinh r a_2^{\text{in}}, \quad (59)$$

$$e^{-i\phi_2} a_2^{\text{out}} = U^\dagger a_2^{\text{in}} U = \cosh r a_2^{\text{in}} - e^{-i\theta} \sinh r a_1^{\text{in}}, \quad (60)$$

where we defined $\cosh(r) = |r_1|$, $\theta = \arg(t_2^* \bar{r}_2)$, and extracted the overall phases $\phi_1 = \arg(r_1)$ and $\phi_2 = \arg(\bar{r}_2)$. Note that the squeezing is hidden in this notation as the antimagnonic operators a_2^{in} and a_2^{out} behave as creation operators. The unitary transformation is given by

$$U = e^{\int_0^\infty d\varepsilon [\xi_{\text{in}}^* a_1^{\text{in}} (a_2^{\text{in}})^\dagger - \xi_{\text{in}} (a_1^{\text{in}})^\dagger a_2^{\text{in}}]} = e^{\int_0^\infty d\varepsilon [\xi_{\text{out}}^* a_1^{\text{out}} (a_2^{\text{out}})^\dagger - \xi_{\text{out}} (a_1^{\text{out}})^\dagger a_2^{\text{out}}]}, \quad (61)$$

where $\xi_{\text{in}} = r e^{i\theta}$ and $\xi_{\text{out}} = r e^{i\theta} e^{i(\phi_L - \phi_R)}$. Then, our vacuum state of no incoming particles $|\Omega\rangle_{\text{in}}$ can be also expressed in terms of the outgoing basis via

$$|\Omega\rangle_{\text{in}} = U |\Omega\rangle_{\text{out}} = \bigotimes_{h_L < \varepsilon < h_R} \frac{1}{|r_1|} \sum_n (-1)^n e^{in(\theta + \phi_L - \phi_R)} \left(\frac{|\bar{t}_1|}{|r_1|} \right)^n |n, n, 0\rangle_{\text{out}}, \quad (62)$$

where $|n_1, n_2, n_3\rangle_{\text{out}}$ is the Fock state for n_i magnons in the i -th out-scattering state. The big circle denotes the continuous tensor product in the relevant energy window $h_L < \varepsilon < h_R$. Beyond that window, the magnon occupation is zero, which we do not write explicitly. From Eq. (62), we identify

$$p_n = \left(1 - \frac{|\bar{t}_1|^2}{|r_1|^2} \right) \left(\frac{|\bar{t}_1|^2}{|r_1|^2} \right)^n, \quad (63)$$

which gives the probability of finding n outgoing magnon-antimagnon pairs at energy ε . The probability follows a geometric probability distribution.

III. MAGNETIC COUPLING TO COLOR CENTERS

Now, we also consider the color centers, which are described by the system Hamiltonian

$$H_S = -\frac{\Delta_L}{\hbar} \cdot \frac{\hbar}{2} \boldsymbol{\sigma}_L - \frac{\Delta_R}{\hbar} \cdot \frac{\hbar}{2} \boldsymbol{\sigma}_R, \quad (64)$$

where we assume $\Delta_{L,R} = (0, 0, \Delta)$ with energy $\Delta > 0$ which can be tuned through an external magnetic field. Thus, energetically both color centers want to point in the $+z$ direction. We denote the basis states of the color centers as $|g,g\rangle, |g,e\rangle, |e,g\rangle$ and $|e,e\rangle$ with g denoting the ground state and e the excited state. Without an environment, the ground state is $|g,g\rangle$ with both color centers pointing in the z -direction. However, the situation changes when we couple the color centers to the stray field of the magnetic environment via the coupling Hamiltonian

$$H_C = -\mathbf{h}_s(\mathbf{r}_L) \cdot \frac{\hbar}{2} \boldsymbol{\sigma}_L - \mathbf{h}_s(\mathbf{r}_R) \cdot \frac{\hbar}{2} \boldsymbol{\sigma}_R, \quad (65)$$

$$= -\frac{\hbar}{2} \sum_{\alpha=L,R} [h_s^+(\mathbf{r}_\alpha) \sigma_\alpha^- + h_s^-(\mathbf{r}_\alpha) \sigma_\alpha^+ + h_s^z(\mathbf{r}_\alpha) \sigma_\alpha^z], \quad (66)$$

where we assume that the color centers are positioned above the environment at distance d on either side of the interface with $\mathbf{r}_\alpha = (x_\alpha, d, 0)$, where $x_L < 0$, $x_R > 0$, and $d > 0$. In the second line, we introduced $h_s^\pm = h_s^x \pm ih_s^y$ and $\sigma_\alpha^\pm = (\sigma_\alpha^x \pm i\sigma_\alpha^y)/2$.

A. Stray magnetic field

The stray field can be calculated via the magnetostatic Greens function $G_V(\mathbf{r} - \mathbf{r}') = -\nabla_{\mathbf{r}} \nabla_{\mathbf{r}'} \frac{\gamma_e^2}{|\mathbf{r} - \mathbf{r}'|}$ [4]

$$\mathbf{h}_s(\mathbf{r}_\alpha) = \int d\mathbf{r}' G_V(\mathbf{r}_\alpha - \mathbf{r}') \mathbf{s}_V(\mathbf{r}') = \int dx' G(x_\alpha - x') \frac{\mathbf{s}(x')}{W}, \quad (67)$$

which fulfills the magnetostatic equation in matter $\nabla \cdot \mathbf{h}_s = -4\pi\gamma_e^2 \nabla \cdot \mathbf{s}_V$ (in Gaussian units; for SI units one has to replace 4π by the vacuum permeability μ_0), where we again included the gyromagnetic ratio γ_e in the definition of \mathbf{h}_s . The spin density per volume is given by

$$\mathbf{s}_V(\mathbf{r}) = \frac{\Theta(|z| - \frac{W}{2})}{W} \delta(y) \mathbf{s}(x), \quad (68)$$

where $\mathbf{s}(x) = [\Theta(-x)\mathbf{s}_L(x) + \Theta(x)\mathbf{s}_R(x)]$ is the spin density per length derived in the scattering theory above. We normalize by W to make $\mathbf{s}_V(\mathbf{r})$ a proper volume density. In the second step of Eq. (67), we introduced the one-dimensional Greens function

$$G(x_\alpha - x') = \int_{-W/2}^{W/2} dz' G_V(x_\alpha - x', -d, -z'). \quad (69)$$

Using the identity $|\mathbf{r}|^{-1} = \int dk_x dk_z e^{-k|y| + ik_x x + ik_z z} / 2\pi k$, we find

$$G(x - x') = -\frac{\gamma_e^2}{2\pi} \int dk_x \int dk_z \frac{e^{-kd + ik_x(x-x')}}{k} W \text{sinc}\left(\frac{k_z W}{2}\right) \begin{pmatrix} k_x^2 & ik_x k_x & k_x k_z \\ ik_x k_x & -k^2 & ik_x k_z \\ k_x k_z & ik_x k_z & k_z^2 \end{pmatrix} \quad (70)$$

$$= -\gamma_e^2 \int dk_x e^{-|k_x|d + ik_x(x-x')} \begin{pmatrix} |k_x| & ik_x & 0 \\ ik_x & -|k_x| & 0 \\ 0 & 0 & 0 \end{pmatrix}, \quad (71)$$

where $k = \sqrt{k_x^2 + k_z^2}$. To get to the second line, we assume the magnetic field of a two-dimensional system $\lim_{W \rightarrow \infty} W \text{sinc}\left(\frac{k_z W}{2}\right) = 2\pi \delta(k_z)$ motivated by the assumption $d \ll W$. Then, we obtain for the stray magnetic field $h_s^\pm = h_s^x \pm ih_s^y$ the expression

$$h_s^\pm(\mathbf{r}_\alpha) = -\frac{2\gamma_e^2}{W} \int_0^\infty dk k e^{-kd} \int dx e^{\mp ik(x_\alpha - x)} s^\mp(x), \quad (72)$$

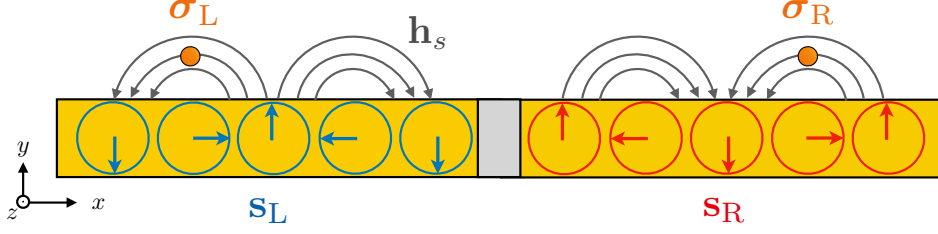


FIG. 6. Snapshot of Halbach-like stray field. On the left, magnons with $k < 0$ create a finite (zero) stray magnetic field above (below) the magnet. On the right, magnons with $k > 0$ create a finite (zero) stray magnetic field above (below) the magnet. By flipping the sign of the magnon wave numbers on either side, the stray field will only be generated below the magnet (not shown). Thus, the coupling to the color centers (orange dots) is chiral. For static magnetic field configurations, this effect is used in a Halbach array [5].

where $s_s^\pm = s_s^x \pm i s_s^y$. Thus, the overall stray field is diluted with $1/W$. Interestingly, the coupling is of a chiral nature, see Fig. 6.

In the following, we assume that $|x_\alpha| \gg d$, such that the left (right) color center only probes the stray field generated by \mathbf{s}_L (\mathbf{s}_R). Then, we obtain

$$h_s^+(\mathbf{r}_L) \approx -\frac{2\gamma_e^2}{W} \sqrt{2\hbar s} \int_0^\infty \frac{d\varepsilon}{\sqrt{2\pi\hbar v_L}} q_L e^{-q_L d} e^{-iq_L x_L} \left(r_1 a_1 + t_2 a_2 \right), \quad (73)$$

$$h_s^+(\mathbf{r}_R) \approx -\frac{2\gamma_e^2}{W} \sqrt{2\hbar s} \int_0^\infty \frac{d\varepsilon}{\sqrt{2\pi\hbar v_R}} \left[\bar{q}_R e^{-\bar{q}_R d} e^{-i\bar{q}_R x_R} \left(\bar{t}_1 a_1 + \bar{r}_2 a_2 \right) + q_R e^{-q_R d} e^{-iq_R x_R} \sqrt{\frac{v_R}{v_R}} r_3^* a_3^\dagger \right], \quad (74)$$

where we neglected the evanescent modes on the left-hand side. Furthermore, also the last term of Eq. (74) will not be important since it does not resonantly couple to the color centers. In particular, the coupling term $h_s^+(\mathbf{r}_R) \sigma_{\bar{R}}^-$ from Eq. (66) gives rise to a strongly oscillating term $a_3^\dagger(\varepsilon) \sigma_- \sim e^{i(\varepsilon+\Delta)t/\hbar}$ with $\varepsilon > 0$ and $\Delta > 0$. Thus, the third scattering state a_3 is irrelevant for the coupling in the secular approximation.

B. Master equation

Integrating out the environment's degrees of freedom, we obtain the master equation

$$\partial_t \rho = \frac{1}{i\hbar} [H_S + \delta H, \rho] + \sum_{i,j=1}^4 \Gamma_{ij} \left(E_i \rho E_j^\dagger - \frac{1}{2} \{E_j^\dagger E_i, \rho\} \right), \quad (75)$$

where δH describes the environment-induced coherent dynamics and Γ the dissipative dynamics. As an operator basis we have chosen $(E_1, E_2, E_3, E_4) = (\sigma_L^+, \sigma_R^+, \sigma_L^-, \sigma_R^-)$. Note that we use the convention that σ_α^+ always increases the spin in the z -direction and, thereby, *lowers* the energy.

1. Dissipative coupling

For the dissipative coupling, we obtain

$$\Gamma = \Gamma_1 \oplus \Gamma_2 = \frac{1}{4} \begin{pmatrix} iG_{LL}^> & iG_{LR}^> & 0 & 0 \\ iG_{RL}^> & iG_{RR}^> & 0 & 0 \\ 0 & 0 & iG_{LL}^< & iG_{RL}^< \\ 0 & 0 & iG_{LR}^< & iG_{RR}^< \end{pmatrix}, \quad (76)$$

where the $1/4$ originates from the coupling Hamiltonian from Eq. (66). The \hbar cancels in the derivation. Then, the decay rates are given by the correlators of the stray magnetic field \mathbf{h}_s in the form of lesser and larger Greens

functions [6]

$$G_{\alpha\beta}^>(\Delta) = -i \int d\tau e^{i\Delta\tau/\hbar} \langle \Omega | h_s^+(\mathbf{r}_\alpha, \tau) h_s^-(\mathbf{r}_\beta) | \Omega \rangle, \quad (77)$$

$$G_{\beta\alpha}^<(\Delta) = -i \int d\tau e^{i\Delta\tau/\hbar} \langle \Omega | h_s^-(\mathbf{r}_\alpha) h_s^+(\mathbf{r}_\beta, \tau) | \Omega \rangle. \quad (78)$$

Note that the full matrix decouples into two 2×2 blocks Γ_1 and Γ_2 which only originate from processes involving the scattering states a_1 and a_2 , respectively. In our case, these blocks can be written in the simple form $\Gamma_1 = \Gamma_0 \boldsymbol{\lambda}_1 \boldsymbol{\lambda}_1^\dagger$ and $\Gamma_2 = \Gamma_0 \boldsymbol{\lambda}_2 \boldsymbol{\lambda}_2^\dagger$ with

$$\boldsymbol{\lambda}_1 = \begin{pmatrix} \sqrt{q_L d} e^{-q_L d} e^{-iq_L x_L r_1} \\ \sqrt{\bar{q}_R d} e^{-\bar{q}_R d} e^{-i\bar{q}_R x_R \bar{t}_1} \end{pmatrix}, \quad \boldsymbol{\lambda}_2 = \begin{pmatrix} \sqrt{q_L d} e^{-q_L d} e^{iq_L x_L t_2^*} \\ \sqrt{\bar{q}_R d} e^{-\bar{q}_R d} e^{i\bar{q}_R x_R \bar{t}_2^*} \end{pmatrix}, \quad (79)$$

where we defined the constant $\Gamma_0 = \frac{\gamma_e^4 \hbar^2 s}{W^2 A d}$ (in Gaussian units). In Eq.(79), all functions are evaluated at energy Δ . As a next step, we eliminate the phases by performing a gauge transformation (rotation around the z -axis) of the form

$$\tilde{\sigma}_L^\pm = e^{\pm i(\arg r_1 - q_L x_L)} \sigma_L^\pm, \quad (80)$$

$$\tilde{\sigma}_R^\pm = e^{\pm i(\arg \bar{t}_1 - \bar{q}_R x_R)} \sigma_R^\pm. \quad (81)$$

By using that $r_1 t_2^* = \bar{r}_2^* \bar{t}_1$, which follows from the properties of the scattering matrix shown in Eq.(56)-(57), we get the real matrices

$$\Gamma_1 = \Gamma_0 d \begin{pmatrix} q_L e^{-2q_L d} r^2 & \sqrt{q_L \bar{q}_R} e^{-(q_L + \bar{q}_R) d} r t \\ \sqrt{q_L \bar{q}_R} e^{-(q_L + \bar{q}_R) d} r t & \bar{q}_R e^{-2\bar{q}_R d} t^2 \end{pmatrix}, \quad (82)$$

$$\Gamma_2 = \Gamma_0 d \begin{pmatrix} q_L e^{-2q_L d} t^2 & \sqrt{q_L \bar{q}_R} e^{-(q_L + \bar{q}_R) d} r t \\ \sqrt{q_L \bar{q}_R} e^{-(q_L + \bar{q}_R) d} r t & \bar{q}_R e^{-2\bar{q}_R d} r^2 \end{pmatrix}, \quad (83)$$

where $r = |r_1| = |\bar{r}_2|$ and $t = |\bar{t}_1| = |t_2|$. Note that the gauge transformation has fully removed the dependence on the position x_α of the color centers.

Since the matrices Γ_1 and Γ_2 are formed by outer products of the vectors $\boldsymbol{\lambda}_1$ and $\boldsymbol{\lambda}_2$, one eigenvalue is always zero. Thus, the diagonalized Lindblad equation has only two relevant Lindblad operators

$$\partial_t \rho = \frac{1}{i\hbar} [H_S + \delta H, \rho] + \sum_{i=1}^2 \Gamma_0 \left(L_i \rho L_i^\dagger - \frac{1}{2} \{L_i^\dagger L_i, \rho\} \right), \quad (84)$$

with

$$L_1 = \sqrt{q_L d} e^{-q_L d} r \tilde{\sigma}_L^+ + \sqrt{\bar{q}_R d} e^{-\bar{q}_R d} t \tilde{\sigma}_R^+ \quad (85)$$

$$L_2 = \sqrt{q_L d} e^{-q_L d} t \tilde{\sigma}_L^- + \sqrt{\bar{q}_R d} e^{-\bar{q}_R d} r \tilde{\sigma}_R^-. \quad (86)$$

We can see already a remarkable effect even in the case where the two magnets of the environment are not coupled ($r = 1$ and $t = 0$). While the left color center does decay to its ground state with $L_1 \propto \sigma_L^+$, the right color center will always transition into its excited state with $L_2 \propto \sigma_R^-$. Thus, the steady state will be $|g, e\rangle$ instead of $|g, g\rangle$. This reflects the fact that the right color center can always emit a negative-energy magnon into the inverted magnet and hence completely reverse its occupation.

2. Coherent coupling

Besides the dissipative coupling, the environment generically also mediates a nonlocal coherent coupling similar to RKKY interaction of the form

$$\delta H = J \sigma_L^+ \sigma_R^- + J^* \sigma_R^+ \sigma_L^-, \quad (87)$$

where

$$J = \frac{1}{4} \Re \mathfrak{c} G_{RL}^R(\Delta). \quad (88)$$

Here we followed Ref. [6] and defined a “real” part of the retarded Greens function which is given by

$$\Re G_{\text{RL}}^{\text{R}}(\Delta) = -i \int d\tau \text{sgn}(\tau) e^{i\Delta\tau/\hbar} \langle \Omega | [h_s^+(\mathbf{r}_R, \tau), h_s^-(\mathbf{r}_L)] | \Omega \rangle = 0, \quad (89)$$

where $\text{sgn}(\tau)$ is the signum function. For our system, we have $[h_s^+(\mathbf{r}_R, \tau), h_s^-(\mathbf{r}_L)] = 0$, where we made use of the relation $r_1 \bar{t}_1^* = t_2 \bar{r}_2^*$ that follows from Eq. (57) for the scattering matrix. Thus, there is no nonlocal coherent coupling between the color centers. There is, however, a local Lamb shift $\propto \delta_\alpha \sigma_\alpha^z$ on either side, which renormalizes the bare energies Δ . This contribution will be ignored in this work as only differences $\delta_L - \delta_R$ will change our results.

C. Entanglement

For the energy $\Delta = (h_L + h_R)/2$, i.e. in the middle of the magnon-antimagnon emission spectrum, we obtain $q_L = \bar{q}_R = q$. Then, the Lindblad operators take on the simple form

$$L_1 = \sqrt{qd} e^{-qd} (r \bar{\sigma}_L^+ + t \bar{\sigma}_R^+), \quad (90)$$

$$L_2 = \sqrt{qd} e^{-qd} (t \bar{\sigma}_L^- + r \bar{\sigma}_R^-). \quad (91)$$

The steady state is pure and has a particularly simple form given by

$$\rho_{\text{st}} = |\psi\rangle\langle\psi|, \quad \text{with} \quad |\psi\rangle = \frac{r |g, e\rangle - t |e, g\rangle}{\sqrt{r^2 + t^2}}. \quad (92)$$

IV. EXCHANGE COUPLING TO COLOR CENTERS

As another example, we consider color centers coupled to the magnets via exchange interaction:

$$H_S = -\frac{\Delta_L}{\hbar} \cdot \frac{\hbar}{2} \boldsymbol{\sigma}_L - \frac{\Delta_R}{\hbar} \cdot \frac{\hbar}{2} \boldsymbol{\sigma}_R \quad (93)$$

$$H_C = -J_X \left[\mathbf{s}_L(x_L) \cdot \frac{\hbar}{2} \boldsymbol{\sigma}_L + \mathbf{s}_R(x_R) \cdot \frac{\hbar}{2} \boldsymbol{\sigma}_R \right] \quad (94)$$

$$= -\frac{\hbar J_X}{2} \sum_{\alpha=L,R} [s_\alpha^+(x_\alpha) \sigma_\alpha^- + s_\alpha^-(x_\alpha) \sigma_\alpha^+ + s_\alpha^z(x_\alpha) \sigma_\alpha^z]. \quad (95)$$

Here, we assume flipped color centers with $\Delta_{L,R} = (0, 0, -\Delta)$ and $\Delta > 0$ such that energetically both color centers want to point in the $-z$ direction. Then, σ_α^+ and σ_α^- increase and decrease the energy, respectively. The second line describes the local exchange interaction parametrized by the exchange coupling J_X . Since the longitudinal fluctuations in s_α^z are of higher order, they are going to be ignored in the following. Carrying out an analogous calculation as in the last section, we find the Lindblad operators

$$L_1 = \frac{1}{\sqrt{q_L \ell}} (e^{iq_L x_L} + r_1 e^{-iq_L x_L}) \sigma_L^- + \frac{1}{\sqrt{\bar{q}_R \ell}} (\bar{t}_1 e^{-i\bar{q}_R x_R}) \sigma_R^- \quad (96)$$

$$L_2 = \frac{1}{\sqrt{q_L \ell}} (t_2 e^{-iq_L x_L})^* \sigma_L^+ + \frac{1}{\sqrt{\bar{q}_R \ell}} (e^{i\bar{q}_R x_R} + \bar{r}_2 e^{-i\bar{q}_R x_R})^* \sigma_R^+, \quad (97)$$

where the rate is now given by $\Gamma_0 = J_X^2 \hbar^2 s \ell / 4A$. In Fig. 7, we show the entanglement of the steady state resulting from these Lindblad operators (where we ignore environment-induced coherent effects from δH). Since the coupling is nonchiral, the spatial dependence on the color centers x_L and x_R survives and entanglement occurs at certain resonances determined by the energy Δ and the positions x_L and x_R . Thus, the chiral nature of the magnetostatic coupling is helpful, but not essential to imprint entanglement onto the color centers.

[1] J. S. Harms, H. Y. Yuan, and R. A. Duine, Antimagnonics, *AIP Advances* **14**, 025303 (2024).

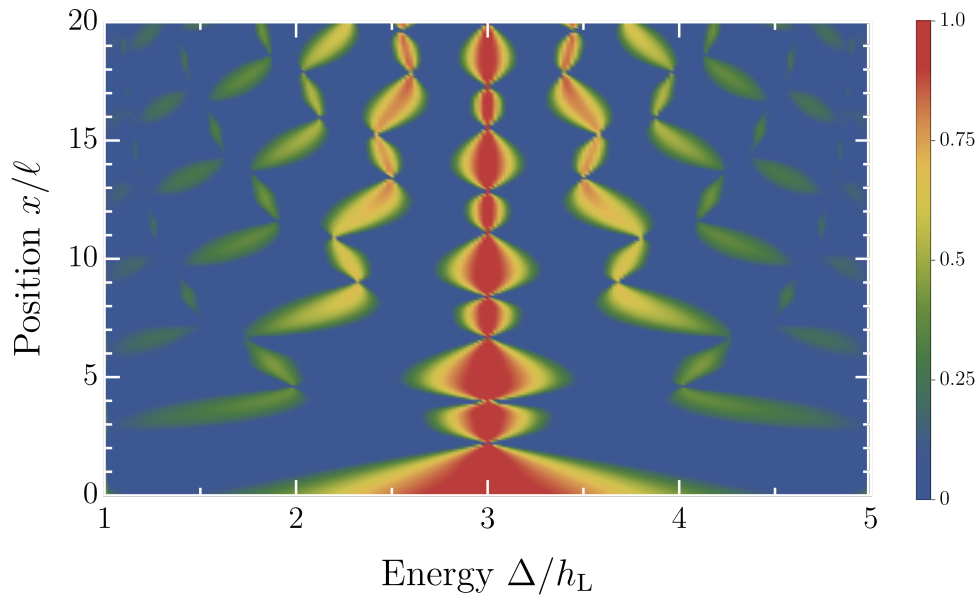


FIG. 7. Steady-state concurrence \mathcal{C} (an entanglement measure) as a function of the color center energy Δ and position $x = -x_L = x_R$. In contrast to the chiral magnetostatic coupling in the Letter, the exchange coupling is nonchiral, and hence a dependence on the color center positions x_L and x_R survives. We choose $h_R = 5h_L$, $\gamma = A/\ell$ and define the length scale $\ell = \sqrt{A/(h_R - h_L)}$.

- [2] R. Balbinot, I. Carusotto, A. Fabbri, C. Mayoral, and A. Recati, Understanding hawking radiation from simple models of atomic bose-einstein condensates, in *Analogue Gravity Phenomenology: Analogue Spacetimes and Horizons, from Theory to Experiment*, edited by D. Faccio, F. Belgiorno, S. Cacciatori, V. Gorini, S. Liberati, and U. Moschella (Springer International Publishing, Cham, 2013) pp. 181–219.
- [3] G. B. Lesovik and I. A. Sadovskyy, Scattering matrix approach to the description of quantum electron transport, *Physics-Uspekhi* **54**, 1007 (2011).
- [4] K. Y. Guslienko and A. N. Slavin, Magnetostatic Green's functions for the description of spin waves in finite rectangular magnetic dots and stripes, *J. Magn. Magn. Mater.* **323**, 2418 (2011).
- [5] K. Halbach, Application of permanent magnets in accelerators and electron storage rings, *Journal of Applied Physics* **57**, 3605 (1985).
- [6] J. Zou, S. Zhang, and Y. Tserkovnyak, Bell-state generation for spin qubits via dissipative coupling, *Phys. Rev. B* **106**, L180406 (2022).